JOURNAL OF AGRICULTURAL AND FOOD CHEMISTRY

pubs.acs.org/JAFC Article

Structurally Diverse Phenolic Amides from the Fruits of *Lycium barbarum* with Potent α-Glucosidase, Dipeptidyl Peptidase-4 Inhibitory, and PPAR-γ Agonistic Activities

Hui Chen,* Wen-Jing Zhang, Jiang-Bo Kong, Yun Liu, Yan-Le Zhi, Yan-Gang Cao, Kun Du, Gui-Min Xue, Meng Li, Zhen-Zhu Zhao, Yan-Jun Sun, Wei-Sheng Feng,* and Zhi-Shen Xie*

Cite This: https://doi.org/10.1021/acs.jafc.3c01669 Read Online

ABSTRACT: A total of nine new phenolic amides (**1**−**9**), including four pairs of enantiomeric mixtures (**3**−**5** and **8**), along with ten known analogues (**10**−**19**) were identified from the fruits of *Lycium barbarum* using bioassay-guided chromatographic fractionation. Their structures were elucidated by comprehensive spectroscopic and spectrometric analyses, chiral HPLC analyses, and quantum NMR, and electronic circular dichroism calculations. Compounds **5**−**7** are the first example of feruloyl tyramine dimers fused through a cyclobutane ring. The activity results indicated that compounds **1**, **11**, and **13**−**17** exhibited remarkable inhibition against α-glucosidase with IC_{50} of 1.11−33.53 μM, 5−150 times stronger than acarbose (IC_{50} = 169.78 μM). Meanwhile, compounds **4a**, **4b**, **5a**, **5b**, **13**, and **14** exerted moderate agonistic activities for peroxisome proliferator-activated receptor (PPAR-γ), with EC_{50} values of 10.09−44.26 μM. Especially,compound **14** also presented inhibitory activity on dipeptidyl peptidase-4 (DPPIV), with an IC_{50} value of 47.13 μM. Furthermore, the banding manner of compounds **14** and **17** with the active site of α-glucosidase, DPPIV, and PPAR-γ was explored by employing molecular docking analysis.

KEYWORDS: *Lycium barbarum, phenolic amides, α-glucosidase inhibitory activity, DPPIV inhibitory activity, PPAR-γ agonistic activity*

INTRODUCTION

Type 2 diabetes mellitus (T2DM) is a complex metabolic disease characterized by insulin resistance and chronic hyperglycemia, which usually progresss with a series of serious chronic complications, such as lipidic abnormality, cardiovascular disease, and hepatic and renal failure.[1,2] In the past two decades, the incidence of T2DM has risen sharply all over the world and has become a serious threat to human health.[3] Over the years, various hypoglycemic agents, including insulin sensitizers (biguanides, thiazolidinediones, TZDs), secretagogues (sulfonylureas, meglitinide), α-glucosidase inhibitors (acarbose), and the latest antidiabetic drugs such as dipeptidyl peptidase-4 (DPPIV) and sodium glucose cotransporter-2 (SGLT2) inhibitors, have been approved for treatment of T2DM.[4,5] However, the prolonged use of these single-target antidiabetic drugs is likely to produce adverse side effects and may also lead to a decline in their efficacy, which limits their clinical applications.[6] Considering the multifaceted pathogenesis of T2DM, discovery and development of multitarget antidiabetic agents may be an efficient therapeutic strategy for the treatment of T2DM.[7] Natural products have served as the source and inspiration for a large number of current drugs. In particular, plants represent a promising source of multitarget antidiabetic leads due to their diverse structures and complex defense mechanisms against diabetes.[8]

Lycium barbarum L. (Solanaceae), a perennial defoliated shrubbery, is generally distributed in the northwest of China.[9] Its fruits, commonly known as "GouQiZi" in Chinese, have been used for centuries as a traditional tonic medicine and functional food for their perceived benefits, including antiaging,[10] antioxidant,[11] neuroprotective,[12] antidiabetic,[13] anticancer, immunomodulatory effects,[14] and so on. Previous phytochemistry investigations on the fruits of *L. barbarum* led to the isolation of polysaccharides, alkaloids, phenylpropanoids, flavonoids, terpenoids, carotenoids, and ascorbic acid derivatives.[15−19] Among them, *L. barbarum* polysaccharides (LBPs) are the most abundant components and have been intensively studied, which were found to have a wide spectrum of bioactivities, including antidiabetic effects.[20,21] Recently, phenolic amides as the predominant alkaloids of this plant, have attracted a great deal of attention due to their diverse structures and significant bioactivities, such as antioxidant,[22] anti-inflammatory,[23] anticancer,[24] and immunomodulatory activities.[25] However, the antidiabetic effects of these phenolic amides isolated from the fruits of *L. barbarum* have rarely been reported.

In a continuing effort to mine bioactive secondary metabolites from the genus *Lycium*,[26,27] the EtOAc extract of *L. barbarum* fruits was found to exhibit significant α-glucosidase inhibition and peroxisome proliferator-activated receptor (PPAR-γ) agonistic activities (Figure 1). Motivated

Received: March 16, 2023
Revised: July 6, 2023
Accepted: July 7, 2023

https://doi.org/10.1021/acs.jafc.3c01669
J. Agric. Food Chem. XXXX, XXX, XXX−XXX

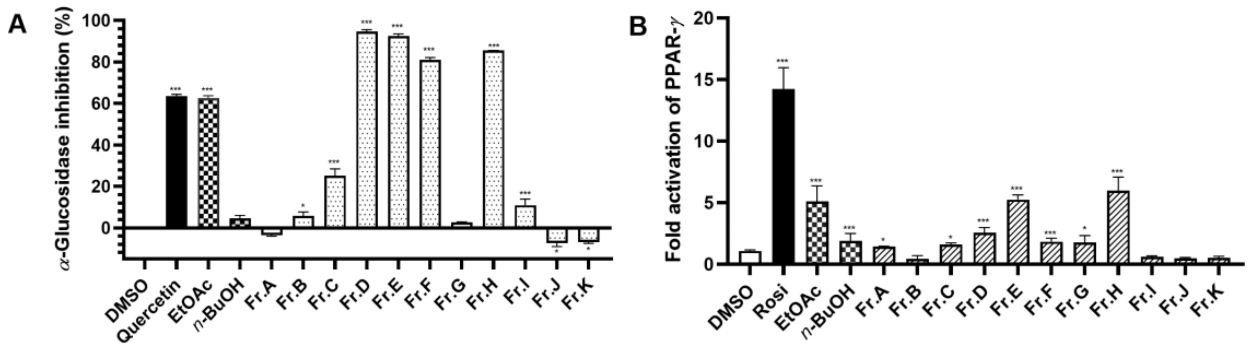

Figure 1. (A) α-glucosidase inhibitory activities of the EtOAc, *n*-BuOH extracts, and different fractions (50 μg/mL). Quercetin is used as positive control with the inhibition of 63.53 ± 0.90% at the test concentration of 10 μM; (B) PPAR-γ agonistic activities of the EtOAc, *n*-BuOH extracts, and different fractions (50 μg/mL). Rosiglitazone (Rosi) is used as the positive control for PPAR-γ, which caused 13.10 ± 1.19-fold activation at the test concentration of 1 μM, and activation by the vehicle (DMSO) was set to 1-fold. Data were expressed as mean ± SD (n = 3). *p < 0.05, **p < 0.01, ***p < 0.001 versus control group.

Table 1. ^{1}H (600 MHz) and ^{13}C NMR (150 MHz) Data of 1 in CD_3OD (δ_H in ppm, J in Hz)

no.	δ_H	δ_C	No.	δ_H	δ_C	no.	δ_H	δ_C
1		127.8	1′		131.0	1″		125.3
2	7.13 d (1.5)	113.4	2′	7.27 d (1.5)	113.4	2″	7.19 d (1.5)	113.4
3		148.9	3′		150.1	3″		149.0
4		150.1	4′		147.5	4″		149.5
5	6.78 d (8.4)	116.5	5′	6.69 d (8.4)	114.7	5″	6.66 d (8.4)	116.1
6	7.03 d (8.4, 1.5)	126.3	6′	6.94 d (8.4, 1.5)	125.9	6″	6.98 dd (8.4, 1.5)	126.4
7	7.82 s	142.2	7′	7.80 s	141.1	7″	7.22 s	125.3
8		126.9	8′		129.5	8″		141.2
9		167.8	9′		167.7	9″		165.4
1‴		131.0	1⁗		130.9	1′′′′′		130.8
2‴, 6‴′	6.82 d (8.4)	130.6	2⁗, 6⁗′	6.82 d (8.3)	130.6	2′′′′′, 6′′′′′	6.72 d (8.4)	130.7
3‴, 5‴′	6.60 d (8.4)	116.2	3⁗, 5⁗′	6.60 d (8.3)	116.2	3′′′′′, 5′′′′′	6.53 d (8.4)	116.2
4‴		156.8	4⁗		156.8	4′′′′′		156.8
7‴	2.39 m	35.4	7⁗	2.45 m	35.4	7′′′′′	2.59 t (7.2)	35.5
8‴	3.20 m	42.9	8⁗	3.32 overlap	42.8	8′′′′′	3.41 t (7.2)	42.2
3-OCH_3	3.69 s	55.9	3′-OCH_3	3.74 s	56.3	3″-OCH_3	3.50 s	56.3

by these findings, we launched a bioactivity-guided isolation of potential antidiabetic compounds from *L. barbarum*. As a result, nine new phenolic amides, lyciumamides O-W (**1**−**9**), and ten known compounds (**10**−**19**) were obtained from the active chromatographic fractions. Herein, we report on their isolation, structural elucidation, and antidiabetic effects on α-glucosidase, DPPIV, and PPAR-γ.

MATERIALS AND METHODS

General Experimental Procedures. Optical rotations were recorded on a Rudolph AP-IV polarimeter. UV and IR spectra were determined using a Thermo EVO 300 and Thermo Nicolet IS 10 spectrometer, respectively. Electronic circular dichroism (ECD) spectra were obtained on an Applied Photophysics Chirascan qCD spectropolarimeter. NMR spectra were acquired using Bruker Avance III 500 and 600 spectrometers. HRESIMS data were recorded on an AB SCIEX TripleTOF 6600 mass spectrometer. Preparative HPLC was carried out using a Sepuruisi LC-52 instrument with an UV200 detector (Beijing Sepurusi scientific Co., Ltd., China) and a YMC-Pack ODS-A column (250 × 20 mm, 5 μm). The column chromatography (CC) was carried out on HP-20 macroporous resin (Mistsubishi Chemical Corporation, Tokyo, Japan), Sephadex LH-20 (Amersham Pharmacia Biotech AB, Sweden), ODS (45−70 μm, Merck), and silica gel (100−200 mesh, Qingdao Marine Chemical Inc. China). TLC was performed on silica gel GF_{254} (Qingdao Marine Chemical, Inc. China).

Plant Material. The fruits of *L. barbarum* were collected from Golmud City, Qinghai Province, China, in September 2017 and authenticated by Prof. Suiqing Chen, School of Pharmacy, Henan University of Chinese Medicine. Its voucher specimen (20170906A) has been deposited in the School of Pharmacy, Henan University of Chinese Medicine, Zhengzhou 450046, China.

Extraction and Isolation. The dried fruits of *L. barbarum* (50 kg) were refluxed with 95% EtOH (200 L, 3 × 2 h). Following the removal of EtOH under reduced pressure, the residue was dispersed in H_2O. The H_2O-solution was chromatographed on an HP-20 macroporous resin column (30 × 120 cm^2) and eluted with H_2O, 95% EtOH, and acetone, respectively. The 95% EtOH extract (1336 g) was suspended in H_2O, followed by successive partitioning with EtOAc and *n*-BuOH to yield EtOAc- (184 g) and *n*-BuOH (386 g)-soluble extracts. The EtOAc extract, exhibiting inhibitory activity against α-glucosidase (62.62% inhibitory rate at a concentration of 50 μg/mL) and PPAR-γ activation (5.12-fold activation at 50 μg/mL) (Figure 1), was subjected to a silica gel CC, eluted with petroleum ether/EtOAc (100:1, 70:1, 50:1, 30:1, 20:1, 10:1, 5:1, and 1:1) and EtOAc/MeOH (30:1, 20:1, 10:1, 5:1, 1:1, 0:1) to afford 11 fractions (A−K) on the basis of TLC analysis. Fractions D−F and H both showed significant inhibition on α-glucosidase (81.02%−94.68% inhibitory rate at 50 μg/mL) and activation of PPAR-γ at a concentration of 50 μg/mL (Figure 1), suggesting that fractions D−F and H of the EtOAc extract might represent the active fractions. Therefore, these four fractions were selected for further purification.

The active fraction D (9.15 g) was chromatographed over Sephadex LH-20 eluting with MeOH to afford the three

https://doi.org/10.1021/acs.jafc.3c01669
J. Agric. Food Chem. XXXX, XXX, XXX−XXX

Table 2. ^{1}H (500 MHz) and ^{13}C NMR (125 MHz) Data of 2−5 in CD_3OD (δ_H in ppm, J in Hz)

	2		3		4		5	
no.	δ_H	δ_C	δ_H	δ_C	δ_H	δ_C	δ_H	δ_C
1	129.7		130.8		130.7			134.5
2	7.31 s	108.1	6.99 d (1.0)	112.2	6.96 d (1.5)	112.6	6.82 d (2.0)	111.6
3		151.3		149.1		148.9		149.1
4		150.0		147.7		147.5		146.6
5	6.94 s	110.4	6.80 d (8.0)	116.0	6.75 d (8.0)	115.7	6.72 d (8.0)	116.2
6		131.3	6.84 dd (8.0, 1.0)	121.6	6.82 d (8.0, 1.5)	122.3	6.67 d (8.0, 2.0)	120.8
7	7.85 s	127.2	4.46 brs	84.3	4.38 d (6.5)	83.7	3.45 d (9.3)	49.6
8		130.9	4.46 brs	85.3	4.50 m	84.9	3.12 d (9.3)	47.9
9		171.3	3.69 dd (10.0, 3.5)	62.2	3.84 d (4.5)	62.3		174.3
			3.49 overlap					
1′		130.5		130.1		130.2		134.5
2′	6.91 d (1.5)	115.4	7.17 d (1.5)	112.3	7.08 d (1.5)	112.3	6.82 d (2.0)	111.6
3′		148.7		151.8		151.8		149.1
4′		147.4		151.7		151.2		146.6
5′	6.90 d (8.0)	116.0	7.01 d (8.5)	117.6	6.89 d (8.0)	117.9	6.72 d (8.0)	116.2
6′	6.80 dd (8.0, 1.5)	124.3	7.06 dd (8.5, 1.5)	122.8	7.01 dd (8.0, 1.5)	122.6	6.67 d (8.0, 2.0)	120.8
7′		137.3	7.46 d (15.5)	141.5	7.42 d (15.5)	141.5	3.45 d (9.3)	49.6
8′		132.5	6.46 d (15.5)	119.9	6.43 d (15.5)	120.0	3.12 d (9.3)	47.9
9′		172.3		169.0		168.9		174.3
1″		131.4		131.3		131.3		131.2
2″, 6″′	7.12 d (8.0)	130.9	7.07 d (8.5)	130.7	7.07 d (8.5)	130.7	6.91 d (8.5)	130.8
3″, 5″′	6.74 d (8.0)	116.3	6.74 d (8.5)	116.3	6.75 d (8.5)	116.3	6.62 d (8.5)	116.2
4″		157.0		157.0		157.0		156.9
7″	2.84 t (7.5)	35.7	2.77 t (7.5)	35.8	2.77 t (7.5)	35.8	2.64 t (7.0)	35.6
8″	3.54 t (7.5)	42.9	3.49 t (7.5)	42.5	3.48 t (7.5)	42.5	3.41 t (7.0),	42.4
							3.26 t (7.0)	
1‴		131.3						131.2
2‴, 6‴′	6.93 d (8.5)	130.5					6.91 d (8.5)	130.8
3‴, 5‴′	6.66 d (8.5)	116.2					6.62 d (8.5)	116.2
4‴		156.8						156.9
7‴	2.27 t (7.5)	35.3					2.64 t (7.0)	35.6
8‴	3.18 t (7.5)	42.8					3.41 t (7.0),	42.4
							3.26 t (7.0)	
3-OCH_3	4.01 s	56.4	3.84 s	54.9	3.80 s	56.4	3.80 s	56.4
7-OCH_3			3.25 s	55.7	3.25 s	57.0		
3′-OCH_3	3.84 s	56.5	3.90 s	55.1	3.80 s	56.5	3.80 s	56.4

corresponding fractions (D_1−D_3). Fraction D_2 (1.26 g) was further fractionated by silica gel CC with petroleum/EtOAc (5:1, 2:1, and 1:1) to yield four subfractions (D_{2-1}−D_{2-4}). Subfraction D_{2-4} (225 mg) was purified by preparative HPLC (60% MeOH/H_2O, 7 mL/min) to yield **16** (15.8 mg, t_R = 42.7 min) and **17** (85.6 mg, t_R = 51.4 min). The bioactive fraction E (25.6 g) was subjected to an ODS column using a gradient of MeOH/H_2O (10:90−90:10) to give nine fractions (E_1−E_9). Fraction E_7 (2.18 g) was applied on a Sephadex LH-20 with MeOH and further purified by preparative HPLC (40% MeOH/H_2O, 7 mL/min) to yield **11** (2.6 mg, t_R 32.0 min), **5** (3.8 mg, t_R 34.0 min), **12** (2.9 mg, t_R 56.0 min), and **10** (1.7 mg, t_R 57.0 min). Fraction F (12.0 g) was subjected to an ODS column eluted with a gradient of MeOH/H_2O (10:90−90:10) to give five fractions (F_1−F_5). Fraction F_3 (3.02 g) was subjected to Sephadex LH-20 CC eluted with MeOH and then further purified by preparative HPLC (35% MeOH/H_2O, 7 mL/min) to afford **6** (1.3 mg, t_R 35.7 min), **7** (2.2 mg, t_R 40.4 min), **8** (2.6 mg, t_R 34.6 min), and **9** (1.8 mg, t_R 48.3 min). Similarly, fraction E_4 (2.58 g) was purified under the same conditions to yield **13** (3.8 mg, t_R 28.2 min), **2** (2.4 mg, t_R 37.2 min), **3** (4.3 mg, t_R 65.1 min), and **4** (5.2 mg, t_R 71.4 min). The active fraction H (7.12 g) was subjected to an ODS column eluted with a gradient of MeOH/H_2O (10:90−90:10) to give six fractions (H_1−H_6). Fraction H_2 (248 mg) was separated by preparative HPLC (47% MeOH/H_2O, 7 mL/min) yielding **1** (2.3 mg, t_R 28.2 min) and **14** (20.5 mg, t_R 39.2 min). Fraction H_3 (352 mg) was purified by preparative HPLC (55% MeCN/H_2O, 7 mL/min) to yield **15** (14.3 mg, t_R 35.1 min), **18** (3.3 mg, t_R 51.4 min), and **19** (5.6 mg, t_R 53.5 min).

Lyciumamide O (1). Yellow gum; UV (MeOH) λ_{max} 224 (4.86), 288 (4.68), 323 (4.74); IR (iTR) ν_{max} 3361, 2924, 1631, 1613, 1513, 1453, 1253, 1133, 1020 cm^{-1}; 1D NMR data (CD_3OD); see Table 1; HRESIMS: m/z 934.3563 $[M - H]^-$ (calcd for $C_{54}H_{52}N_3O_{12}$, 934.3556).

Lyciumamide P (2). Yellow amorphous powder; UV (MeOH) λ_{max} 208 (4.47), 225 (4.45), 254 (4.47), 278 (4.17); IR (iTR) ν_{max} 3327, 2935, 1633, 1613, 1513, 1438, 1257, 1028, 828 cm^{-1}; 1D NMR data (CD_3OD); see Table 2; HRESIMS: m/z 645.2202 $[M + Na]^+$ (calcd for $C_{36}H_{34}N_2O_8Na$, 645.2207).

(±)-Lyciumamide Q (3). White amorphous powder; UV (MeOH) λ_{max} 207 (4.21), 223 (4.11), 286 (3.97), 318 (3.94); IR (iTR) ν_{max} 3361, 2925, 1651, 1596, 1511, 1453, 1260, 1032 cm^{-1}; 1D NMR data (CD_3OD); see Table 2; HRESIMS: m/z 546.2099 $[M + Na]^+$ (calcd for $C_{29}H_{33}NO_8Na$, 546.2098).

(+)-Lyciumamide Q (3a). White amorphous powder; $[\alpha]_D^{25}$ = +14.2 (c 0.02, CH_3OH); ECD (CH_3OH) λ_{max} ($\Delta\varepsilon$): 206 (0.18), 216 (0.13), 231 (0.24), 264 (0.00), 274 (0.03), 304 (−0.02), 335 (0.06), 366 (−0.01), 389(0.03), 397 (0.00) nm.

https://doi.org/10.1021/acs.jafc.3c01669
J. Agric. Food Chem. XXXX, XXX, XXX−XXX

Table 3. ^{1}H and ^{13}C NMR Data of Compounds 6−9 (δ_H in ppm, J in Hz)

	6[a]		7[b]		8[b]		9[b]	
no.	δ_H	δ_C	δ_H	δ_C	δ_H	δ_C	δ_H	δ_C
1		131.3		132.5		130.9		133.2
2	6.86 s	112.5	6.80 d (1.8)	111.9	7.08 d (1.8)	111.2	6.99 d (1.8)	111.1
3		146.9		148.7		148.7		149.1
4		145.0		146.0		147.3		147.6
5	6.68 d (8.3)	114.8	6.72 d (8.4)	115.9	6.78 d (8.0)	115.7	6.80 d (8.2)	116.3
6	6.64	120.0	6.66 dd (8.4, 1.8)	120.8	6.85 d (8.0, 1.8)	120.2	6.87 d (8.2, 1.8)	120.2
7	4.13 dd (10.0, 7.5)	40.4	3.89 t (9.0)	42.8	5.54 d (5.4)	84.9	5.32 dd (5.0, 2.1)	84.2
8	3.66 dd (10.0, 7.5)	47.2	3.61 t (8.4)	50.9	3.48 dd (6.6, 5.4)	57.0	3.16 dd (5.0, 2.1)	58.1
9		170.7		172.9		171.6		172.2
1′		131.3		132.5		135.0		133.2
2′	6.86 s	112.5	6.80 d (1.8)	111.9	7.02 d (1.8)	111.0	6.99 d (1.8)	111.1
3′		146.9		148.7		149.2		149.1
4′		145.0		146.0		147.5		147.6
5′	6.68 d (8.3)	114.8	6.72 d (8.4)	115.9	6.76 d (8.0)	116.3	6.80 d (8.2)	116.3
6′	6.64	120.0	6.66 dd (8.4, 1.8)	120.8	6.86 d (8.0, 1.8)	120.4	6.87 d (8.2, 1.8)	120.2
7′	4.13 dd (9.9, 7.5)	40.4	3.89 t (9.0)	42.8	5.84 d (9.0)	83.3	5.32 dd (5.0, 2.1)	84.2
8′	3.66 dd (9.9, 7.5)	47.2	4.21 t (10.2)	49.6	3.43 dd (9.0, 6.6)	58.7	3.16 dd (5.0, 2.1)	58.1
9′		170.7		175.7		171.5		172.2
1″		129.5		131.4		131.3		131.2
2″, 6″′	6.78 d (8.2)	129.2	6.89 d (8.4)	130.6	6.92 d (8.4)	130.7	6.91 d (8.5)	130.7
3″, 5″′	6.61 d (8.2)	115.0	6.60 d (8.4)	116.1	6.67 d (8.4)	116.3	6.65 d (8.5)	116.2
4″		155.5		156.7		156.9		156.9
7″	2.18 t (7.6)	34.3	2.23 t (7.2)	35.7	2.60 t (7.2)	35.6	2.62 m	35.7
8″	3.02 m, 2.86 m	40.4	2.97 t (7.2)	42.0	3.34 overlap	42.4	3.38 m	42.5
					3.29 overlap		3.20 m	
1‴		129.5		131.2		131.3		131.2
2‴, 6″″	6.78 d (8.2)	129.2	6.71 d (8.4)	130.8	6.83 d (8.5)	130.5	6.91 d (8.5)	130.7
3‴, 5″″	6.61 d (8.2)	115.0	6.59 d (8.4)	116.2	6.65 d (8.5)	116.2	6.65 d (8.5)	116.2
4‴		155.5		156.8		156.8		156.9
7‴	2.18 t (7.6)	34.3	2.68 t (7.2)	35.6	2.22 t (7.2)	35.5	2.62 m	35.7
8‴	3.02 m, 2.86 m	40.4	3.44 t (7.2)	42.5	3.36 m	42.1	3.38 m	42.5
					3.29 m		3.20 m	
3-OCH_3	3.76 s	55.6	3.81 s	56.4	3.86 s	56.4	3.84 s	56.4
3′-OCH_3	3.76 s	55.6	3.81 s	56.4	3.84 s	56.4	3.84 s	56.4

[a]Measured in DMSO-d_6; ^{1}H NMR for 500 MHz, ^{13}C NMR for 125 MHz. [b]Measured in CD_3OD; ^{1}H NMR for 600 MHz, ^{13}C NMR for 150 MHz.

*(−)-Lyciumamide Q (**3b**).* White amorphous powder; $[\alpha]_D^{25}$ = −13.5 (*c* 0.02, CH_3OH); ECD (CH_3OH) λ_{max} ($\Delta\varepsilon$): 204 (−0.29), 214 (−0.18), 233 (−0.32), 262 (−0.05), 274 (−0.07), 306 (−0.03), 318 (−0.09), 374 (−0.02), 388(0.05), 397 (−0.01) nm.

*(±)-Lyciumamide R (**4**).* White amorphous powder; UV (MeOH) λ_{max} 208 (4.32), 223 (4.26), 286 (4.11), 320 (4.08); IR (iTR) ν_{max} 3358, 2923, 1652, 1596, 1512, 1454, 1261, 1033 cm^{-1}; 1D NMR data (CD_3OD); see Table 2; HRESIMS: *m*/*z* 522.2139 $[M - H]^-$ (calcd for $C_{29}H_{32}NO_8$, 522.2133).

*(+)-Lyciumamide R (**4a**).* White amorphous powder; $[\alpha]_D^{25}$ = +18.3 (*c* 0.02, CH_3OH); ECD (CH_3OH) λ_{max} ($\Delta\varepsilon$): 191 (−0.05), 193 (−0.15), 215 (0.23), 226 (0.10), 238 (0.29), 267 (0.06), 288 (0.09), 342 (−0.04), 360 (0.02), 382 (−0.03), 398 (0.00) nm.

*(−)-Lyciumamide R (**4b**).* White amorphous powder; $[\alpha]_D^{25}$ = −18.6 (*c* 0.02, CH_3OH); ECD (CH_3OH) λ_{max} ($\Delta\varepsilon$): 192 (−0.24), 201 (0.33), 214 (−0.18), 226 (−0.01), 240 (−0.32), 266 (−0.05), 290 (−0.09), 329 (0.05), 346 (0.00), 376 (0.03), 397 (0.00) nm.

*(±)-Lyciumamide S (**5**).* White amorphous powder; UV (MeOH) λ_{max} 208 (4.58), 224 (4.31), 282 (3.82); IR (iTR) ν_{max} 3316, 2924, 1636, 1516, 1512, 1454, 1244, 1017 cm^{-1}; 1D NMR data (CD_3OD); see Table 2; HRESIMS: *m*/*z* 649.2521 $[M + Na]^+$ (calcd for $C_{36}H_{38}N_2O_8Na$, 649.2520).

*(−)-Lyciumamide S (**5a**).* White amorphous powder; $[\alpha]_D^{25}$ = −19.7 (*c* 0.01, CH_3OH); ECD (CH_3OH) λ_{max} ($\Delta\varepsilon$): 207 (2.01), 230 (−0.32), 245 (0.67), 273 (0.03), 288 (0.48), 303 (0.07), 316 (0.03), 328 (0.11), 380 (0.03) nm.

*(+)-Lyciumamide S (**5b**).* White amorphous powder; $[\alpha]_D^{25}$ = +21.4 (*c* 0.01, CH_3OH); ECD (CH_3OH) λ_{max} ($\Delta\varepsilon$): 207 (−1.76), 231 (0.37), 245 (−0.63), 273 (−0.02), 290 (−0.44), 304 (−0.04), 316 (−0.08), 326 (−0.01), 374 (−0.04) nm.

*Lyciumamide T (**6**).* White amorphous powder; UV (MeOH) λ_{max} 208 (4.60), 223 (4.31), 280 (3.84); IR (iTR) ν_{max} 3316, 2924, 1636, 1516, 1512, 1454, 1244, 1017 cm^{-1}; 1D NMR data (DMSO-d_6); see Table 3; HRESIMS: *m*/*z* 649.2509 $[M + Na]^+$ (calcd for $C_{36}H_{38}N_2O_8Na$, 649.2520).

*Lyciumamide U (**7**).* White amorphous powder; UV (MeOH) λ_{max} 206 (4.58), 224 (4.31), 281 (3.82); 1D NMR data (CD_3OD); see Table 3; HRESIMS: *m*/*z* 649.2503 $[M + Na]^+$ (calcd for $C_{36}H_{38}N_2O_8Na$, 649.2520).

*(±)-Lyciumamide V (**8**).* White amorphous powder; UV (MeOH) λ_{max} 208 (4.58), 226 (4.31), 280 (3.82); IR (iTR) ν_{max} 3387, 2922, 1651, 1611, 1515, 1453, 1236, 1032 cm^{-1}; 1D NMR data (CD_3OD); see Table 3; HRESIMS: *m*/*z* 665.2452 $[M + Na]^+$ (calcd for $C_{36}H_{38}N_2O_9Na$, 665.2470).

*(−)-Lyciumamide V (**8a**).* White amorphous powder; $[\alpha]_D^{25}$ = −27.5 (*c* 0.02, CH_3OH); ECD (CH_3OH) λ_{max} ($\Delta\varepsilon$): 209 (−5.31), 222 (−1.53), 236 (−2.16), 258 (−0.07), 285 (−0.21), 388 (0.06) nm.

https://doi.org/10.1021/acs.jafc.3c01669
J. Agric. Food Chem. XXXX, XXX, XXX−XXX

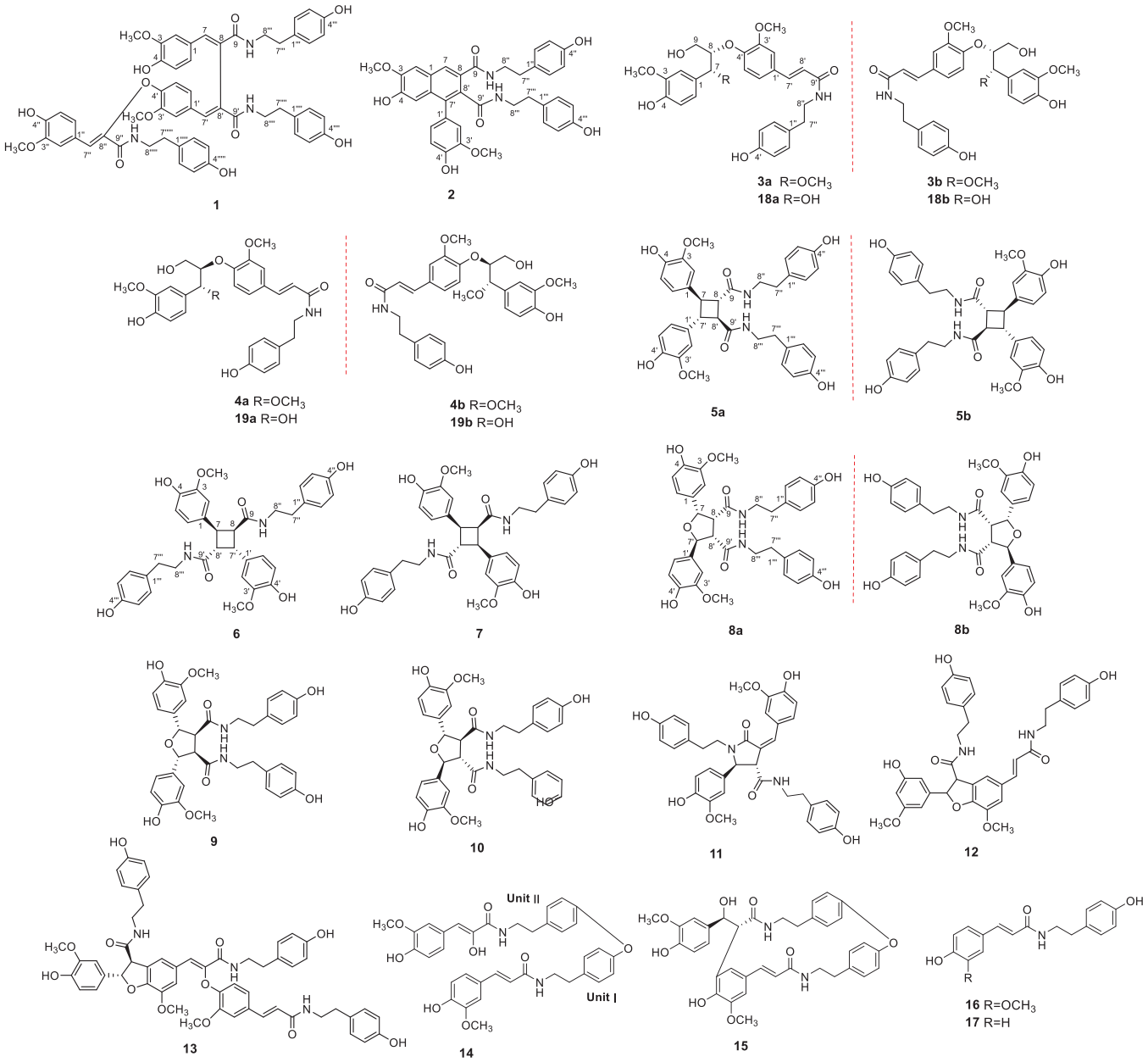

Figure 2. Structures of compounds **1**−**19**.

*(+)-Lyciumamide V (**8b**)*. White amorphous powder; $[\alpha]_D^{25}$ = +33.8 (*c* 0.03, CH_3OH); ECD (CH_3OH) λ_{max} ($\Delta\varepsilon$): 209 (5.33), 222 (1.41), 236 (2.16), 261 (−0.02), 284 (0.20), 385 (0.02) nm.

*Lyciumamide W (**9**)*. White amorphous powder; UV (MeOH) λ_{max} 208 (4.57), 226 (4.30), 280 (3.80); 1D NMR data (CD_3OD); see Table 3; HRESIMS: *m*/*z* 665.2457 $[M + Na]^+$ (caled for $C_{36}H_{38}N_2O_9Na$, 665.2470).

α-Glucosidase Inhibitory Activity. The α-glucosidase inhibitory activity was performed using 4-nitrophenol-α-D-glucopyranoside (PNPG) according to the reported protocols.[28] α-Glucosidase from *Saccharomyces cerevisiae* was purchased from Sigma-Aldrich (St. Louis, Mo, U.S.A.). Briefly, the extract, fractions, and compounds were dissolved in 0.5% DMSO and then diluted with phosphate buffer. α-Glucosidase solution (0.025 U/mL), PNPG (1 μM), test compounds (50 μM), extract, and fractions (50 μg/mL) were mixed and incubated in 96-well plates at 37 °C for 50 min. Thereafter, the absorbance was measured at 405 nm by using a microplate reader, and the inhibition rate of α-glucosidase activity was calculated. Quercetin and acarbose were selected as the positive control. Test methods for IC_{50} values of the compounds were the same as above. The purities of compounds submitted to bioassay are more than 95%.

DPPIV Inhibitory Activity. The DPPIV inhibitory activity was performed as previously described.[29] Recombinant human DPPIV was purchased from Cayman Chemical (Ann Arbor, MI, U.S.A.). In brief, a mixture of 10 μL of sample (dissolved in DMSO), 10 μL of DPPIV enzyme (10 mg/L, dissolved in Tris-HCl buffer), and 70 μL of Tris-HCl buffer was added to a 96-well plate and incubated at 37 °C for 10 min, and then the reaction began after 10 μL of substrate solution was added. 100 μL of $NaHCO_3$ (0.1 M) was used to stop the reaction, and the absorbance was measured at 405 nm. Sitagliptin was used as a positive control. The inhibition rate and IC_{50} values were calculated by using the previous formula.

PPAR-γ Agonistic Activity Assay. The PPAR-γ activity assay was performed as previously described.[30] HEK293T cells were seeded at a density of 2 × 10^4 cells per well into 96-well plates for 18 h and transfected over a 6 h period with 50 ng of plasmid Psg5-PPAR-γ, 50 ng of the PPAR promoter-reporter vector J3-TKLuc expressed target genes, and 10 ng of β-galactosidase reporter to normalize transfection efficiencies using PolyJet DNA in vitro transfection reagents

https://doi.org/10.1021/acs.jafc.3c01669
J. Agric. Food Chem. XXXX, XXX, XXX−XXX

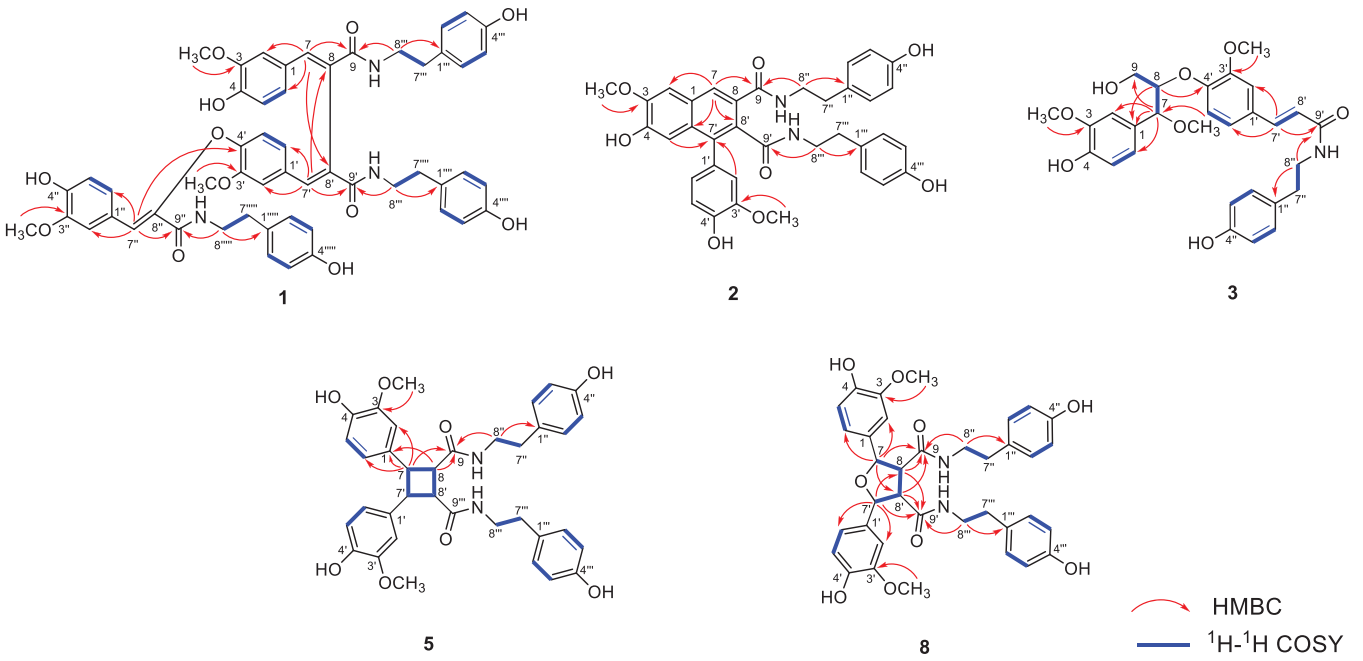

Figure 3. Key 2D NMR correlations of compounds **1**−**3**, **5**, and **8**.

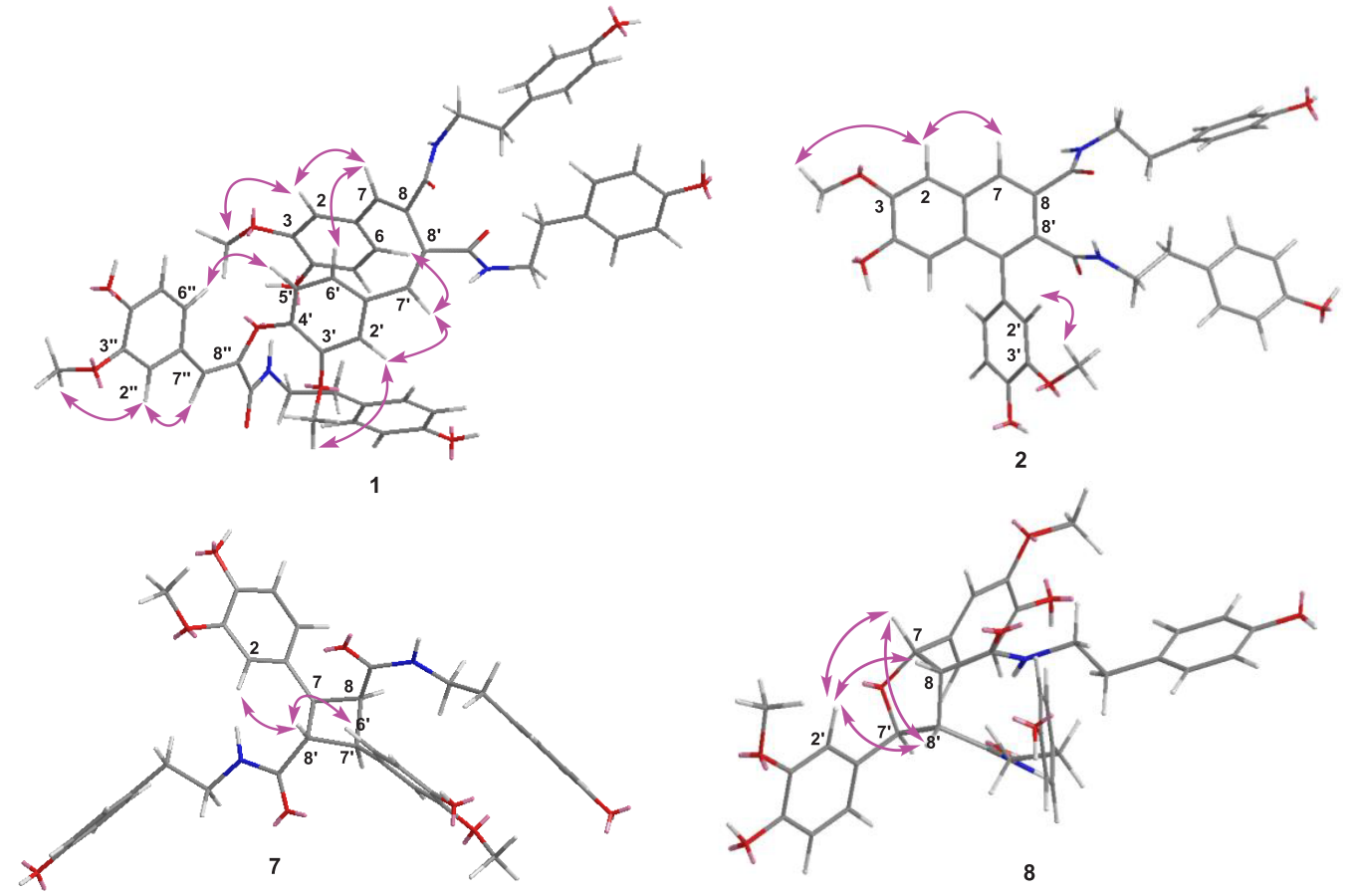

Figure 4. Key NOESY correlations of compounds **1**, **2**, **7**, and **8**.

(SignaGen, U.S.A). Then, the cells were treated with the extracts, fractions, and compounds. Rosiglitazone (RSG) was used as a positive control. The luciferase reporter assay kit (Promega, U.S.A) was used to measure the luciferase activity.

https://doi.org/10.1021/acs.jafc.3c01669
J. Agric. Food Chem. XXXX, XXX, XXX−XXX

Scheme 1. Hypothetical Biogenetic Pathways of Compounds 1−9

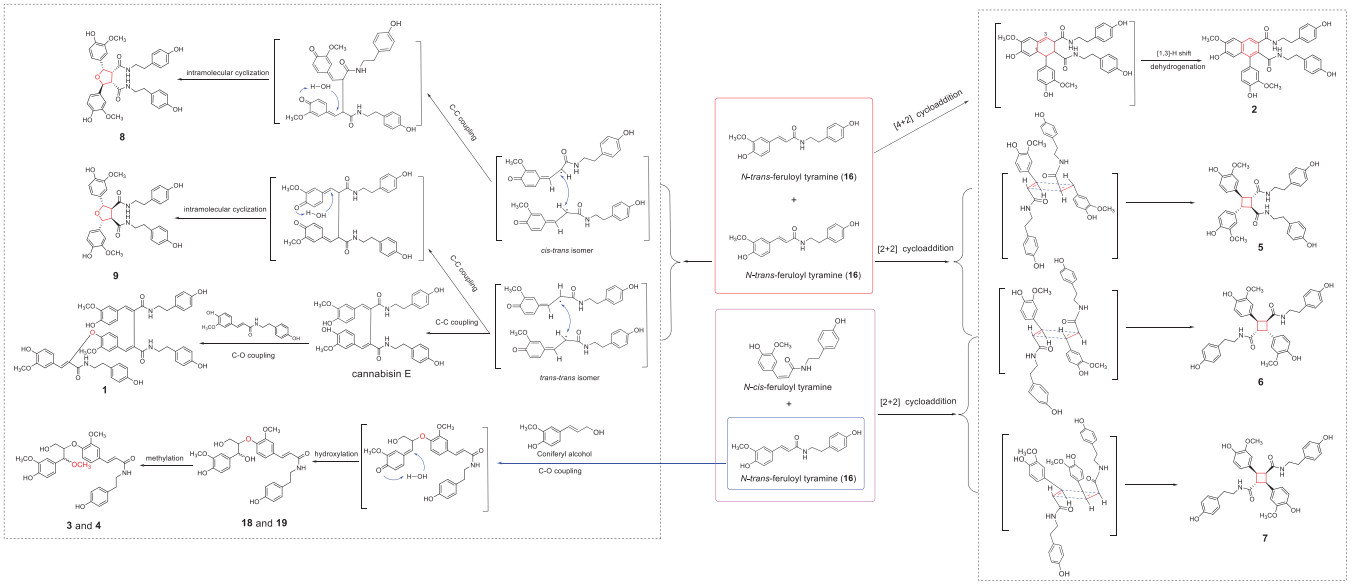

Molecular Docking. All computational analyses were performed using Schrödinger Maestro 2015. The crystallographic structures of α-glucosidase, DPPIV, and PPAR-γ were obtained from the Protein Data Bank (PDB code 1OBB, 4A5S, and 4CI5, respectively), and the image files were generated using pymol 2.4. Compounds **14**, **17**, acarbose, sitagliptin, and rosiglitazone were prepared by using the ligand preparation wizard in Maestro with standard settings. Grids of α-glucosidase, DPPIV, and PPAR-γ were generated using Glide, following the standard procedure recommended by Schrödinger.

RESULTS AND DISCUSSION

Structure Elucidation of Compounds 1−9. Lyciumamide O (**1**) was obtained as a yellow gum. The molecular formula of **1** was assigned as $C_{54}H_{53}N_3O_{12}$ on the basis of HRESIMS data at *m/z* 934.3563 $[M - H]^-$, suggesting 30 degrees of unsaturation. The UV spectrum of **1** showed absorption bands at 224, 288, and 323 nm. The presence of hydroxy and conjugated carbonyl groups in **1** was revealed by the bands at 3361 and 1631 cm^{-1}, respectively. Analysis of the ^1H, and ^{13}C NMR data (Table 1) of **1** revealed the presence of three tyramine moieties (C-1‴−C-8‴, C-1⁗−C-8⁗, and C-1⁗′−C-8⁗′), three 1,3,4-trisubstituted aromatic moieties, and three trisubstituted double bonds. In addition, the resonances due to three carbonyl carbons (δ_C 167.8, 167.7, and 165.4) and three methoxy groups were also observed. These data together with the molecular formula ($C_{54}H_{53}N_3O_{12}$) were consistent with *N-trans*-feruloyl tyramine (**16**) trimer. The HMBC correlations (Figure 3) of H-7 to C-2, C-6, C-9, and C-8′, and H-7′ to C-8, C-2′, C-6′, and C-9′ indicate the presence of two *N-trans*-feruloyl tyramine groups were connected between the C-8 and C-8′ positions, which was constructed as a cannabisin D-like unit in this molecule.[31] The 8″-*O*-4′ linkage between the last *N-trans*-feruloyl tyramine group and the cannabisin D-like unit was determined by the $^3J_{CH}$ HMBC correlations of H-7″ to C-2‴, C-6‴, and C-9‴ and the key $^4J_{CH}$ HMBC correlation of H-7″ to C-4′ (Figures 3 and S7), as well as the downfield chemical shift of C-8″ (δ_C 141.2) and the NOESY correlations of H-6″/H-5′ (Figure 4). The *E* relation at the double bond of the three feruloyl tyramine moieties was confirmed by the NOESY correlations of H-2/H-7, H-7/H-6′, H-6/H-7′, H-2′/H-7′, H-2″/H-7‴, and H-6‴/H-5′. Furthermore, the three methoxy groups were attached to C-3, C-3′, and C-3‴, respectively, as suggested by HMBC correlations of 3-OCH_3/C-3, 3′-OCH_3/C-3′, and 3″-OCH_3 to C-3″, in combination with the NOESY interactions and biogenetic consideration (Scheme 1).

Lyciumamide P (**2**) was obtained as a yellow, amorphous powder, and its molecular formula was deduced to be $C_{36}H_{34}N_2O_8$ from the HRESIMS ion peak at *m/z* 645.2202 $[M + Na]^+$, corresponding to 21 degrees of unsaturation. The UV spectrum of **2** revealed absorption bands at 208, 225, 254, and 278 nm. IR absorptions for hydroxy (3327 cm^{-1}), conjugated carbonyl (1633 cm^{-1}), and aromatic rings (1613 and 1513 cm^{-1}) were also observed. The ^1H NMR spectrum of **2** (Table 2) showed the presence of two *p*-tyramine moieties [δ_H 7.12 (2H, d, *J* = 8.0 Hz, H-2″, 6‴), δ_H 6.74 (2H, d, *J* = 8.0 Hz, H-3″, 5‴), 3.54 (2H, t, *J* = 7.5 Hz, H-8″), 2.84 (2H, t, *J* = 7.5 Hz, H-7″); δ_H 6.93 (2H, d, *J* = 8.5 Hz, H-2⁗, 6⁗), δ_H 6.66 (2H, d, *J* = 8.5 Hz, H-3⁗, 5⁗), 3.18 (2H, t, *J* = 7.5 Hz, H-8⁗), 2.27 (2H, t, *J* = 7.6 Hz, H-7⁗)] that are typical groups in most lignanamides. In addition, one 1,3,4-trisubstituted aromatic moiety [δ_H 6.91 (1H, d, *J* = 1.5 Hz, H-2′), 6.90 (1H, d, *J* = 8.0 Hz, H-5′), 6.80 (1H, dd, *J* = 8.0, 1.5 Hz, H-6′)], one 1,2,4,5-tetrasubstituted aromatic moiety [δ_H 7.31 (1H, s, H-2), 6.94 (1H, s, H-5)], one pentasubstituted aromatic moiety [δ_H 7.85 (1H, s, H-7)], and two methoxy groups [δ_H 4.01 (3H, s) and 3.84 (3H, s)] were also observed in the ^1H NMR spectrum. These results were also supported by the ^{13}C NMR spectrum, with 36 carbon signals; these were sorted by DEPT experiments, including two conjugated carbonyl carbons (δ_C 172.3 and 171.3), 24 aromatic carbons (δ_C 157.0 to δ_C 108.1), four methylenes (δ_C 42.9, 42.8, 35.7, and 35.3), and two methoxy carbons (δ_C 56.5 and 56.4). Careful analysis of the one-dimensional NMR results (^1H, ^{13}C) of **2** resembled those of lyciumamide N,[23] except for two additional methoxy groups at C-3 and C-3′ respectively in **2**. Therefore, compound **2** was suggested to be an arynaphthalene-type lignanamide, comprising two feruloyl tyramine moieties.[32] The connectivities of **2** were further determined by HSQC and HMBC experiments (Figure 3). In particular, the HMBC correlations from 3-OCH_3 (δ_H 4.01) to C-3 (δ_C 151.3), and 3′-OCH_3 (δ_H 3.84) to

https://doi.org/10.1021/acs.jafc.3c01669
J. Agric. Food Chem. XXXX, XXX, XXX−XXX

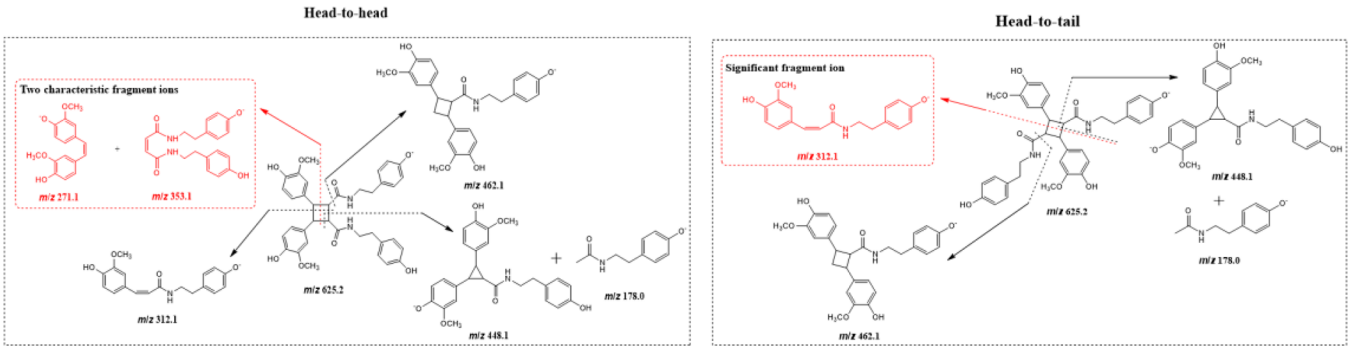

Figure 5. Major fragments observed in the ESIMS^2 of **5**−**7**.

C-3′ (δ_C 148.7), along with the NOESY correlations of H-7/H-2, H-2/3-OCH_3, and H-2′/3′-OCH_3 (Figure 4) further confirmed the location of the two methoxy groups.

(±)-Lyciumamide Q (**3**) was obtained as a white, amorphous powder. The HRESIMS $[M + Na]^+$ ion m/z 546.2099 established its elemental formula as $C_{29}H_{33}NO_8$. The ^1H and ^{13}C NMR spectra (Table 2) of **3** showed the presence of the characteristic signals of one *N-trans*-feruloyl tyramine unit (C-1′−C-9′ and C-1″−C-8″). Additionally, two oxymethine, one oxymethylene, and three methoxy groups were also observed in the NMR spectra. The $^1H-^1H$ COSY correlations of H-7/H-8/H-9, together with the HMBC correlations for H-7/C-1, C-2, C-6, C-9, H-8/C-1 and C-4′ (Figure 3) revealed the 8-*O*-4′ linage in **3**. The NMR data of **3** were similar to those of (7,8-*erythro*)-1-(4-hydroxy-3-methoxyphenyl)-2-{4-{2-[*N*-2-(4-hydroxyphenyl)ethyl]-carbamoylehenyl-2-methoxyphenoxyl}}-1,3-propanodiol-named (**18**),[33] except that the hydroxy group at C-7 in **18** was replaced by a methoxy group in **3**. This structural variation was confirmed by the key HMBC correlation of 7-OCH_3/C-7. The 7,8-*erythro* configuration of **3** was established on the basis of the small coupling constants between H-7 and H-8 ($J \approx 0$ Hz), which was identical to the published data and conformational analysis results (Figure S123, Supporting Information).[33−35] In addition, the $\Delta\delta_{C8-C7}$ were successfully applicable to distinguish the *erythro* and *threo* aryl glycerol units in the different series of 8-*O*-4′ neolignan derivatives.[33,36] The $\Delta\delta_{C8-C7}$ value of the *erythro* **3** (1.0 ppm) was smaller than those of **4** (1.2 ppm), which was also consistent with data reported in the literature.[33] The lack of optical activity and weak CD Cotton effects in the ECD spectrum indicated that **3** was a racemic mixture. Subsequent chiral HPLC separation on a Chiralpak AD-H column was carried out, and it finally gave two optically pure enantiomers, **3a** and **3b** (Figure S89, Supporting Information), which exhibited mirror-image-like ECD curves and opposite specific rotations. By comparison of their ECD data (Figure S31, Supporting Information) with those of (7*R*,8*S*)-**18** and (7*S*,8*R*)-**18**,[33] the absolute configurations of **3a** and **3b** were defined as 7*R*,8*S* and 7*S*,8*R*, respectively.

(±)-Lyciumamide R (**4**) had the same molecular formula ($C_{29}H_{33}NO_8$) as **3**, as deduced from the HRESIMS data at m/z 522.2139 $[M - H]^-$. Analysis of the NMR data (Table 2) of **4** indicated that it was an epimer of **3**, due to their closely similar spectroscopic features. The large coupling constant between H-7 and H-8 (J = 6.5 Hz) and larger $\Delta\delta_{C8-C7}$ value suggested a relative *threo* configuration of **4**.[33,34] Similarly, **4** was also a racemic mixture and was separated by chiral HPLC into two enantiomers, **4a** and **4b**. (Figure S90, Supporting Information). The absolute configurations of **4a** and **4b** were then assigned as 7*R*,8*R* and 7*S*,8*S*, respectively, by comparing their experimental ECD data (Figure S40, Supporting Information) with those of (7*R*,8*R*)-**19** and (7*S*,8*S*)-**19**.[33]

(±)-Lyciumamide S (**5**) was obtained as a white, amorphous powder. Its molecular formula was established as $C_{36}H_{38}N_2O_8$ from the $[M + Na]^+$ peak at m/z 649.2521 in HRESIMS, indicating 19 degrees of unsaturation. The IR absorptions at 3316, 1636, and 1516 cm^{-1} suggested the presence of hydroxy-, carbonyl-, and aromatic ring functionalities. The NMR data (Table 2) of **5** displayed characteristic signals similar to those of *N-trans*-feruloyl tyramine (**16**), with the absence of an olefinic pair in the data of **5**; conversely, signals for two additional methine units [δ_H 3.45 (1H, d, J = 9.3 Hz), δ_C 49.6; δ_H 3.12 (1H, d, J = 9.3 Hz), δ_C 47.9] were observed. These ^1H and ^{13}C NMR data accounted for only half the number of signals expected for its molecular formula ($C_{36}H_{34}N_2O_8$), indicating that **5** was a dimer of **16** fused through a cyclobutane ring, which was further confirmed by the $^1H-^1H$ COSY and HMBC spectra (Figure 3). Two different types of dimerization patterns, head-to-head and head-to-tail, are possible for **5**, and they are easily distinguished by the presence of two additional MS fragment ions at m/z 353.1 and 271.1 only observed in head-to-head cyclization molecules (Figure 5).[37] In the MS^2 spectrum of **5**, these two characteristic fragment ions at m/z 353.1500 and 271.0972 were detected (Figure S48, Supporting Information), indicating that **5** possesses a head-to-head fused cyclobutane ring. Consideration the symmetry of this molecule, there are four possible relative configurations of the cyclobutane ring: all *trans* (**5-I**), all *cis* (**5-II**), 7/8-*trans*, 7′/8′-*trans*, 8/8′-*cis* (**5-III**), or 7/8-*cis*, 7′/8′-*cis*, 8/8′-*trans* (**5-IV**) (Figure S97, Supporting Information). The possibility of an all-*cis* form was excluded based on a distinct NOESY cross-peak of H-2/H-8 (Figure S46, Supporting Information). However, due to the symmetry of the cyclobutane ring, the remaining three possible isomers (**5-I**, **5-III**, and **5-IV**) could not be distinguished by NOESY correlations. By observing almost identical $^3J_{H\text{-}7,7'/8,8'}$ values of **5** (9.3 Hz) with those of cyclobutane-containing chalcone dimer, oxyfadichalcone C (9.0 Hz; all *trans*) but not with those of oxyfadichalcone B (6.0 Hz; 7/8-*trans*, 7′/8′-*trans*, 8/8′-*cis*),[38] the relative configuration of **5** was thus assigned as all *trans*. To further confirm above conclusion, the NMR calculations of four isomers, **5-I**-**5-IV**, were also carried out by the gauge independent atomic orbital (GIAO) method at the mPW1PW91/6-311+G(2d,p) level.[27] The results showed that the line correlation coefficient (R^2) value between the

https://doi.org/10.1021/acs.jafc.3c01669
J. Agric. Food Chem. XXXX, XXX, XXX−XXX

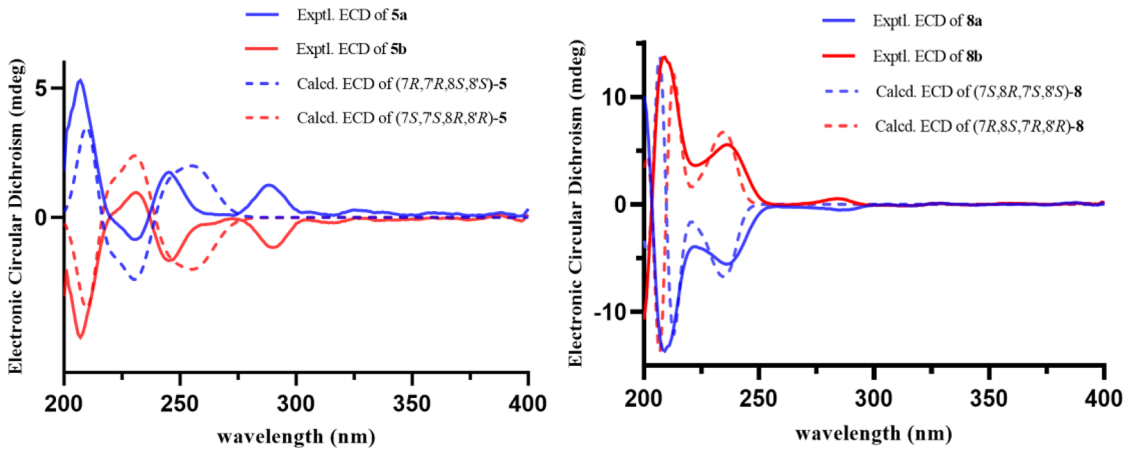

Figure 6. Calculated and experimental ECD spectra of **5a**/**5b** and **8a**/**8b** in MeOH.

experimental and calculated ^{13}C NMR data for **5-II** (R^2 = 0.9970) was lower than the values computed for the three remaining isomers (0.9982 for **5-I**; 0.9984 for **5-III**; 0.9985 for **5-IV**), which was consistent with the above NOESY analysis results. To further distinguish among **5-I**, **5-III**, and **5-IV**, the parameter of DP4+ probability analysis was performed for the combination of ^{1}H and ^{13}C NMR data. As a result, the DP4+ probability of **5-I** was 100%, indicating that an all *trans* form (**5-I**) was the most probable relative configuration of the cyclobutane ring. Compound **5** was also racemic, inferred from its almost zero specific rotation and weak Cotton effects. The isolation of individual enantiomers (**5a** and **5b**) was accomplished by chiral HPLC (Figure S91, Supporting Information), and the absolute configuration of **5a** and **5b** were assigned as 7*R*,7′*R*,8*S*,8′*S* and 7*S*,7′*S*,8*R*,8′*R*, respectively, based on comparison of their experimental and calculated ECD spectra (Figure 6).

Lyciumamide T (**6**) was assigned the same molecular formula as **5**, as determined from its HRESIMS data at *m*/*z* 649.2509 $[M + Na]^+$. The UV, IR, and NMR (Table 3) spectra were similar to those of **5**, indicating **6** also to be a symmetric feruloyl tyramine dimer fused through a cyclobutane ring. In the MS^2 spectrum of **6**, the characteristic fragment ions disappeared at *m*/*z* 353.1 and 271.1 and the presence of significant fragment ion at *m*/*z* 312.1230, indicating that **6** was a dimeric cycloadduct connected in a head-to-tail manner (Figure S59, Supporting Information). Three possible relative configurations, 7/8-*cis*, 7′/8′-*cis*, 8/8′-*trans* (**6a**), all *trans* (**6b**), and all *cis* (**6c**), are possible for **6**. The NOESY cross-peak of H-2/H-8 provided evidence for the exclusion of the last one (Figure S57, Supporting Information). The relative configuration of the cyclobutane ring in **6** was assigned as 7/8-*cis*, 7′/8′-*cis*, 8/8′-*trans* based on the $J_{H\text{-}7,7'/8,8'}$ values (10.0, 7.5 Hz), which was in a good agreement with those of oxyfadichalcone A (10.5, 6.5 Hz; 7/8-*cis*, 7′/8′-*cis*, 7/8′-*trans*).[38] Furthermore, the NMR data of two possible isomers, **6a** and **6b**, were also calculated using the same method as that for **5** (Figure S101, Supporting Information). The results showed that the calculated NMR data of **6a** were in good accordance with the experimental values with a high DP4+ probability of 100% (Figure S104, Supporting Information). Interestingly, the structure of **6** was a mesomer due to the existence of a symmetry center in the molecule (Figure S125, Supporting Information) and thus lacks optical activity and Cotton effects in its ECD spectrum.

The data accumulated for lyciumamide U (**7**) showed that it has the same molecular formula as **5** and **6**. Compound **7** was also found to be a cyclobutane-containing feruloyl tyramine dimer derived from a head-to-tail [2 + 2] cyclization based on its MS^2 (Figure S64, Supporting Information) and NMR spectra data. Unlike the above point symmetry dimers, the ^{1}H and ^{13}C NMR spectra (Table 3) of **7** displayed well-resolved resonances for two tyramine moieties and two methines of cyclobutane methines [δ_H 4.21 (1H, t, *J* = 10.2 Hz, H-8′), 3.61 (1H, t, *J* = 8.4 Hz, H-8); δ_C 50.9 (C-8), 49.6 (C-8′)], as well as the superimposed resonances for two sets of 1,3,4-trisubstitued phenyl rings and the remaining cyclobutane methines [δ_H 3.89 (2H, t, *J* = 9.0 Hz, H-7, 7′); δ_C 42.8 (C-7, 7′)], which are indicative of a plane symmetry dimer.[38] Consideration on the plane symmetry of this molecule, there is only one possible relative configuration of the cyclobutane ring, which is shown in Figure 2. This result was further confirmed by the diagnostic NOESY correlations of H-8′/H-2 and H-8′/H-6′ in conjunction with the absence of an NOE interaction of H-8/H-8′ (Figure 4). Compound **7** was also centrosymmetric and thus lacks optical activity and Cotton effects in its ECD spectrum.

(±)-Lyciumamide V (**8**) was obtained as a white, amorphous powder, and its molecular formula of $C_{36}H_{38}N_2O_9$ was determined by the HRESIMS ion peak at *m*/*z* 665.2452 $[M + Na]^+$, corresponding to 19 degrees of unsaturation. IR analyses confirmed the presence of hydroxy (3387 cm^{-1}) and carbonyl (1651 cm^{-1}) groups. The ^{1}H and ^{13}C NMR spectra (Table 3) of **8** showed the signals of two *p*-tyramine moieties, two 1,3,4-trisubstituted aromatic moieties, two carbonyl carbons, four methines, and two methoxy groups. The characteristic ^{13}C NMR resonances at δ_C 84.9 (C-7), 83.3 (C-7′), 58.7 (C-8′), and 57.0 (C-8) suggested the presence of a tetrahydrofuran ring, which was further confirmed by the $^{1}H-^{1}H$ COSY correlations of H-7/H-8/H-8′/H-7′ and key HMBC correlations of H-7 to C-8′ and H-7′ to C-8 (Figure 3). Further HMBC correlations of H-7 to C-2, C-6, C-9, H-8 to C-9 and C-9′, H-7′ to C-2′, C-6′, C-9′, and H-8′ to C-9′ and C-9 established the position of the tetrahydrofuran ring, which was connected to phenyl groups at C-7 and C-7′ and tyramine groups at C-8 and C-8′. The NOESY correlations of H-7/H-8′, H-7/H-2′, H-2′/H-8, and H-2′/H-8′, but no correlation of H-7/H-7′ (Figure 4), defined the relative configuration of the tetrahydrofuran ring as 7/8-*cis*, 8/8′-*cis*, 7′/8′-*trans*. In fact, the coupling constants of H-7′/H-8′ (9.0 Hz) and H-7/H-8 (5.4 Hz), which were corresponding to

https://doi.org/10.1021/acs.jafc.3c01669
J. Agric. Food Chem. XXXX, XXX, XXX−XXX

those of bisavenanthramide B-5, a dimeric compound of avenanthramide phytoalexin in oats.[39] **8** was also analyzed and separated by chiral HPLC to yield two enantiomeric isomers **8a** and **8b** (Figure S92, Supporting Information). The absolute configurations of **8a** and **8b** were, respectively, determined as 7*S*,8*R*,7′*S*,8′*S* and 7*R*,8*S*,7′*R*,8′*R* by comparison of their experimental and calculated ECD spectra (Figure 6).

Lyciumamide W (**9**) had the same molecular formula as **8**, $C_{36}H_{38}N_2O_9$, deduced from its HRESIMS data at *m*/*z* 665.2457 $[M + Na]^+$. Interestingly, only one set of signals could be observed in the ^1H and ^{13}C NMR spectra (Table 3) of compound **9**, indicating that this compound possesses a symmetric structure. The ^1H and ^{13}C NMR data (Table 3) as well as 2D NMR correlations (Figures S83−S86, Supporting Information) indicated that the structure of **9** was highly similar to that of lyciumamide K (**10**),[40] a symmetrical feruloyl tyramine dimer fused through a tetrahydrofuran moiety isolated from *L. yunnanense* Kuang, with the minor differences caused by the ^{13}C NMR shifts of C-7/7′ (δ_C 84.2 for **9**; δ_C 86.2 for **10**) and C-8/8′ (δ_C 58.1 for **9**; δ_C 60.6 for **10**), which revealed that these two compounds have an identical gross structure. Given the molecular symmetry, four possible relative configurations of the tetrahydrofuran ring could be constructed: 7/8-*cis*, 7′/8′-*cis*, 8/8′-*trans* (**9a**), 7/8-*trans*, 7′/8′-*trans*,8/8′-*cis* (**9b**), all *trans* (**9c**), and all *cis* (**9d**) (Figure S99, Supporting Information). The possibility of an all *trans* form could be first ruled out because its structure was identical to those of **10**, and the possibility of an all-*cis* form was also excluded based on distinct NOE cross-peaks of H-2/H-8 and H-6/8 in the NOESY spectrum of **9** (Figure S86, Supporting Information). Thus, only two possible relative configurations, **9a** and **9b**, were left to be determined. To further distinguish between **9a** and **9b**, the computationally calculated NMR data of the two possible diastereomers were also compared to the experimental data for **9**. The result indicated that **9b** matches well with the experimental data with a high probability of 100% (Figures S102 and S105, Supporting Information). The structure of **9** was also a mesomer and did not show apparent Cotton effects in its ECD spectrum.

The other ten known compounds were identified as lyciumamide K (**10**),[40] heliotropamide (**11**),[41] tribulusamide A (**12**),[42] cannabisin O (**13**),[43] lyciumamide A (**14**),[22] lyciumamide B (**15**),[22] *N*-*E*-feruloyl tyramine (**16**),[22] *N*-*E*-coumaroyl tyramine (**17**),[22] (7, 8-*erythro*)-1-(4-hydroxy-3-methoxyphenyl)-2-{4-{2-[*N*-2-(4-hydroxyphenyl)ethyl]-carbamoylehenyl-2-methoxyphenoxyl}}-1,3-propanodiol-named (**18**),[33] (7, 8- *threo*)-1-(4-hydroxy-3-methoxyphenyl)-2-{4-{2-[*N*-2-(4-hydroxyphenyl)ethyl]carbamoylehenyl-2-methoxyphenoxyl}}-1,3-propanodiolnamed (**19**)[33] by comparing the spectroscopic data from the isolated compounds with the data reported in the literature.

Hypothetical Biogenetic Pathways of Compounds 1−9. Structurally, compound **1** is a rare trimeric feruloyl tyramine isolated from the *Lycium* species, compounds **5**−**7** represent the first example of naturally occurring feruloyl tyramine dimers fused through a cyclobutane ring, while compounds **8** and **9** are the second example of feruloyl tyramine dimers fused through a tetrahydrofuran ring following after the first example compound **10** from the *Lycium* species. Inspired by their structural characteristics, a putative biosynthetic pathway for **1**−**9** is proposed in Scheme 1. The two phenolic amide monomers, *N*-*trans*-feruloyl tyramines (**16**) and its *cis*-isomer, *N*-*cis*-feruloyl tyramine, which are derived from the amino acids of tryptophan and tyrosine,[44,45] were considered as the biosynthetic precursors of **1**−**9**. Briefly, compounds **1**, **3**, **4**, **8**, and **9** could be formed from **16** via the key biosynthetic steps of radical−radical coupling (8−8′ C−C and/or 8-*O*-4′ C−O coupling), hydroxylation, and/or intramolecular cyclization reactions according to the biosynthesis of lignan.[46,47] For compounds **2**, **5**, **6**, and **7**, the cycloaddition reactions ([4 + 2] and/or [4 + 2] cycloaddition) were proposed to play an important role in the construction of the arynaphthalene and tetrahydrofuran scaffolds, which was inspired by the biosynthesis of some cyclobutene-type norlignans and dimeric stibenes cycloaddition.[48,49]

Evaluation of Biological Activities. All of the isolated compounds, except for the racemic mixtures of **3**−**5** and **8**, were assayed for their α-glucosidase inhibitory activity. Compounds **1**, **11**, and **13**−**17** showed remarkable inhibition of α-glucosidase at a concentration of 50 μM, and their dose−response relationships were further studied to provide their respective IC_{50} values (Table 4). The phenolic amide trimers (**1** and **13**) and dimers (**11**, **14**, and **15**) displayed high activity on α-glucosidase with IC_{50} values ranging from 12.49 to 33.53 μM, which were much more potent than the positive control acarbose (IC_{50} = 169.78 μM). Notably, the *N*-*E*-coumaroyl tyramine monomer (**17**) demonstrated the most potent α-glucosidase inhibitory activity (IC_{50} = 1.11 μM), which was superior to that of its 3-methoxy substituted derivative (**16**, IC_{50} = 4.63 μM), and its dimers and trimers. The results revealed that the *N*-*E*-coumaroyl tyramine fragment was a key factor for the α-glucosidase inhibitory activity, and this conclusion is consistent with previous observations.[50] In contrast, the introduction of the 3-methoxy group as in **16** and formation of its dimers and trimers weakened the activity.

Table 4. α-Glucosidase Inhibitory Activities[a]

	α-glucosidase	
compounds	inhibition rate at 50 μM (%)	IC_{50} (μM)
1	97.55 ± 0.60	17.46 ± 0.62
11	52.20 ± 1.97	33.53 ± 1.83
13	97.05 ± 0.58	12.49 ± 1.85
14	86.05 ± 2.20	12.65 ± 0.49
15	96.50 ± 0.24	23.42 ± 0.13
16	95.17 ± 0.12	4.63 ± 0.58
17	96.52 ± 0.08	1.11 ± 0.02
acarbose[b]	NT[c]	169.78 ± 7.41

[a]Values are expressed as the mean ± SD (*n* = 3). [b]Acarbose is used as the positive control for α-glucosidase inhibitory assay. [c]NT: not test.

In addition to α-glucosidase inhibitory activity, compounds **12**−**14**, **16**, and **17** were further evaluated for their inhibition of DPPIV and sitagliptin as a positive control. Compound **14**, a phenolic amide dimer consisting of *N*-*E*-feruloyl tyramine unit (unit I) and a unit of its 8-hydroxy substituted derivative (unit II), showed moderate inhibition (50.99%, 50 μM) with an IC_{50} value of 47.13 ± 0.87 μM. In contrast, the other compounds (**12**, **13**, **16**, and **17**) only had weak activity with the inhibition of 12.68%, 24.90%, 31.23%, and 18.75%, respectively, at the test concentration of 50 μM. When comparing to **14**, the phenolic amide monomers **16** and **17** exhibited obviously decreased activity indicating the importance of unit II for the potency of DPPIV.

Furthermore, these compounds, except for the racemic mixtures of **3**−**5** and **8**, were also assessed for their agonistic

https://doi.org/10.1021/acs.jafc.3c01669
J. Agric. Food Chem. XXXX, XXX, XXX−XXX

Table 5. PPAR-γ Agonistic Activities[a]

compounds	EC_{50} (μM)
4a	32.69 ± 2.17
4b	44.26 ± 1.44
5a	15.62 ± 1.12
5b	27.42 ± 1.35
13	42.83 ± 1.72
14	10.09 ± 0.93
rosiglitazone[b]	0.129 ± 0.05

[a]Values are expressed as the mean ± SD (n = 3). [b]Rosiglitazone is used as the positive control for the PPAR-γ agonistic assay.

activity on PPAR-γ. Compounds **4a**, **4b**, **5a**, **5b**, **13**, and **14** showed moderate agonistic activities for PPAR-γ with EC_{50} values ranging from 10.09 to 44.26 μM (Table 5). It was noticeable that the phenolic amide dimer (**14**) showed the most potent agonistic activity with an EC_{50} value of 10.09 μM, while the phenolic amide monomers (**16** and **17**) did not show PPAR-γ agonistic activity. This finding suggested that the 8-hydroxy substituted unit also plays a crucial role in PPAR-γ agonistic activity. In addition, enantiomers **4a** and **4b**, which both had a 7,8-*threo* configuration, exhibited moderate PPAR-γ agonistic activities. In contrast, compounds **3a** and **3b**, both having a 7,8-*threo* configuration, exhibited no PPAR-γ agonistic effect. Similarly, compounds **5a** and **5b**, both having a *trans* form configuration in the cyclobutane ring, displayed better activity than **6** and **7** (with a 7,8-*cis* configuration). It can be concluded that 7,8-*threo* or all *trans* form configuration in the structure of 8-*O*-4′ linkage or cyclobutane type phenolic amides might enhance the PPAR-γ agonistic effect.

Molecular Docking Analysis. To better understand the experimental results, a molecular docking study was conducted to simulate the interactions of active compounds with α-glucosidase (PDB code 1OBB). Compounds **14** and **17**, which respectively represent the monomeric and dimeric phenolic amide scaffolds, both showed an obvious α-glucosidase inhibitory effect, were selected for the molecular modeling using the program. The docking protocol was validated reproducing the binding mode of acarbose at the catalytic domain. As shown in Figure 7, both compounds **14** and **17** could bind with the catalytic pocket of α-glucosidase with the interactions of hydrogen-bond. It is noted that compound **17** formed three stable hydrogen-bond interactions between the two *p*-hydroxy and C-9 carbonyl groups of **17** and key amino acid residues of α-glucosidase that may be responsible for the high activity, whereas only two hydrogen-bond interactions were detected in unit I of **14** probably because of the disappearance of the *p*-hydroxy group at C-4‴ and the induction of the methoxy group at C-3′. Interestingly, unit II of **14**, which differs from unit I in having a hydroxy group at C-8, showed no hydrogen-bond interactions with α-glucosidase, indicating that the presence of 8-hydroxy unit II could reduce the inhibitory activity against α-glucosidase. The docking results further corroborated the importance of the *N*-*E*-coumaroyl tyramine fragment for the inhibition of α-glucosidase. The residues involved in the binding as well as the type of interactions are summarized in Table S6 and Figures S106−S112 in the Supporting Information.

In addition, docking analysis of compound **14** using the crystallized structure of DPPIV (PDB code 4A5S) and PPAR-γ (PDB code 4CI5) was also performed, which was validated with sitagliptin and rosiglitazone, respectively (Tables S7−S8 and Figures S113−S122, Supporting Information). Different from the α-glucosidase docking results, both units of **14** displayed significant hydrogen-bond interactions or $\pi-\pi$ stacking interaction with key amino acid residues of DPPIV and PPAR-γ. For the DPPIV docking results (Figure 8A,B),

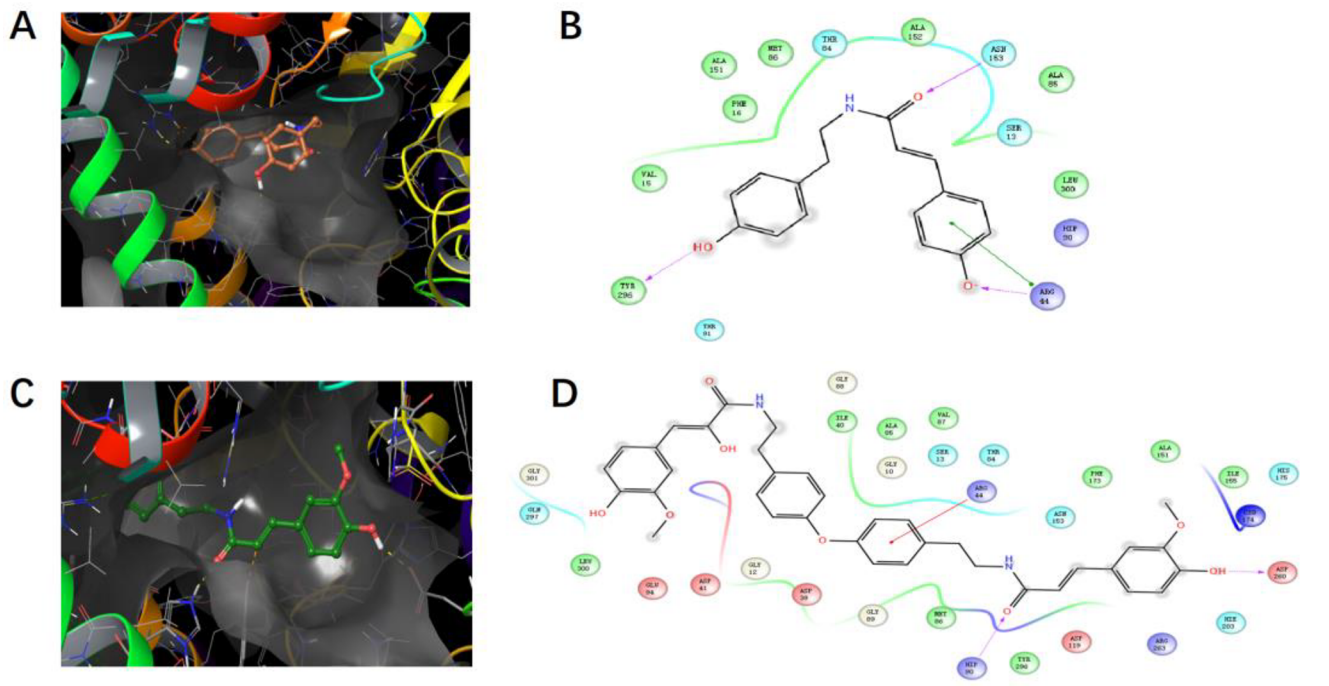

Figure 7. 3D ligand-interaction diagram of compounds **14** (A) and **17** (C) into the α-glucosidase pocket; 2D ligand-interaction diagram of compounds **14** (B) and **17** (D) into the α-glucosidase pocket. (B/D) H-bonds are depicted with purple arrows−dashed arrows for H-bonds involving the amino acid side chain and regular arrows for H-bonds involving the amino acid backbone.

https://doi.org/10.1021/acs.jafc.3c01669
J. Agric. Food Chem. XXXX, XXX, XXX−XXX

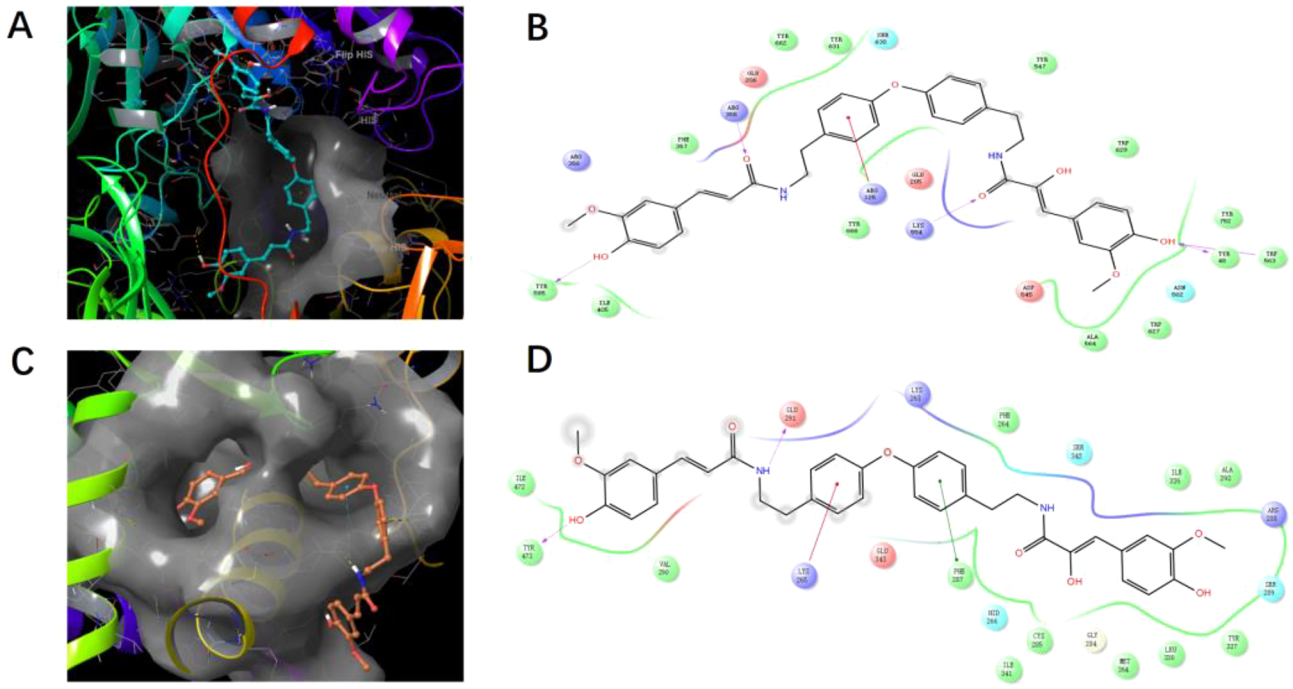

Figure 8. Docking analysis of compound **14** with DPPIV (A/B) and PPAR-γ (C/D). (B/D) H-bonds are depicted with purple arrows−dashed arrows for H-bonds involving amino acid side chain and regular arrows for H-bonds involving amino acid backbone. Straight green lines represent π-stacking interactions.

the C-4′ hydroxy and C-9′ carbonyl groups of unit I of **14** formed two hydrogen-bonding interactions with Tyr585 and Arg358. On the other hand, the C-4 hydroxy and C-9 carbonyl groups of unit II of **14** also formed three hydrogen-bonding interactions with Trp563, Tyr48, and Lys554. For the PPAR-γ docking results (Figure 8C,D), the C-4′ hydroxy and the amino groups of unit I formed two strong hydrogen-bonding interactions with Tyr473 and Glu291. Furthermore, $\pi-\pi$ stacking interaction was observed between unit II of **14** and the residue of Phe287. The docking results revealed that both units of **14** play a crucial role in controlling the DPPIV inhibitory and PPAR-γ agonistic activities.

In conclusion, in this work, a total of 19 compounds, including nine new phenolic amides, were obtained from the fruits of *L. barbarum* under a bioactivity-guided isolation procedure. In addition, most of the isolates were evaluated for their antidiabetic potential *in vitro* using α-glucosidase, DPPIV, and PPAR-γ as targets, and several compounds displayed potent α-glucosidase inhibitory and/or PPAR-γ agonistic effects. The DPPIV inhibitory and PPAR-γ agonistic activities of these compounds are reported for the first time. Notably, two monomeric phenolic amide alkaloids (**16** and **17**) exhibited more potent α-glucosidase inhibitory effects than the positive control, acarbose. Especially, the dimeric amide alkaloid (**14**) demonstrated dual inhibitory activities against α-glucosidase and DPPIV, and also PPAR-γ agonistic activity, which highlighted its potential as the leading compound for the development of multitargeted agents for the treatment of T2DM. Furthermore, results from molecular docking further confirmed the good interaction of compounds **14** and **17** with α-glucosidase and/or DPPIV/PPAR-γ. Taken together, these findings enrich the structural diversity of alkaloids in *L. barbarum* and also provide a basis for development and utilization of phenolic amides derivatives as a source of anti-T2DM agents from medicinal and edible plants.

■ ASSOCIATED CONTENT

Supporting Information

The Supporting Information is available free of charge at https://pubs.acs.org/doi/10.1021/acs.jafc.3c01669.

1D and 2D NMR spectra, HRESIMS spectra, and UV spectra of compounds **1**−**9**; IR spectra of compounds **1**−**6** and **8**; ECD spectra and Chiral HPLC Separation of compounds **3**−**5** and **8**; ECD calculations of compounds **5** and **8**, NMR calculation of compounds **5**, **6**, and **9**, and molecular docking analysis of **14** and **17** (PDF)

■ AUTHOR INFORMATION

Corresponding Authors

Hui Chen − *School of Pharmacy, Henan University of Chinese Medicine, Zhengzhou 450046, P. R. China; Co-Construction Collaborative Innovation Center for Chinese Medicine and Respiratory Diseases by Henan & Education Ministry of P. R. China, Zhengzhou 450046, P. R. China;* orcid.org/0000-0002-5648-3449; Email: chenhuiyxy@hactcm.edu.cn

Wei-Sheng Feng − *School of Pharmacy, Henan University of Chinese Medicine, Zhengzhou 450046, P. R. China; Co-Construction Collaborative Innovation Center for Chinese Medicine and Respiratory Diseases by Henan & Education Ministry of P. R. China, Zhengzhou 450046, P. R. China;* orcid.org/0000-0002-5987-412X; Email: fwsh@hactcm.edu.cn

Zhi-Shen Xie − *Academy of Chinese Medical Sciences, Henan University of Chinese Medicine, Zhengzhou 450046, P. R. China*; Email: xiezhishen@hactcm.edu.cn

Authors

Wen-Jing Zhang − *School of Pharmacy, Henan University of Chinese Medicine, Zhengzhou 450046, P. R. China*

https://doi.org/10.1021/acs.jafc.3c01669
J. Agric. Food Chem. XXXX, XXX, XXX−XXX

Jiang-Bo Kong − *School of Pharmacy, Henan University of Chinese Medicine, Zhengzhou 450046, P. R. China*
Yun Liu − *School of Pharmacy, Henan University of Chinese Medicine, Zhengzhou 450046, P. R. China*
Yan-Le Zhi − *School of Pharmacy, Henan University of Chinese Medicine, Zhengzhou 450046, P. R. China;* orcid.org/0000-0001-6066-2231
Yan-Gang Cao − *School of Pharmacy, Henan University of Chinese Medicine, Zhengzhou 450046, P. R. China*
Kun Du − *School of Pharmacy, Henan University of Chinese Medicine, Zhengzhou 450046, P. R. China*
Gui-Min Xue − *School of Pharmacy, Henan University of Chinese Medicine, Zhengzhou 450046, P. R. China*
Meng Li − *School of Pharmacy, Henan University of Chinese Medicine, Zhengzhou 450046, P. R. China*
Zhen-Zhu Zhao − *School of Pharmacy, Henan University of Chinese Medicine, Zhengzhou 450046, P. R. China;* orcid.org/0000-0001-7961-4694
Yan-Jun Sun − *School of Pharmacy, Henan University of Chinese Medicine, Zhengzhou 450046, P. R. China; Co-Construction Collaborative Innovation Center for Chinese Medicine and Respiratory Diseases by Henan & Education Ministry of P. R. China, Zhengzhou 450046, P. R. China*

Complete contact information is available at: https://pubs.acs.org/10.1021/acs.jafc.3c01669

Funding

This research work was financially supported by the National Natural Science Foundation of China (Grants 22177027 and 21602047) and the Key Projects for Science and Technology Development of Henan (232102310441), Science & Technology Innovation Talents in Universities of Henan Province (22HASTIT048), and Training Program for Young Backbone Teachers in Higher Education Institutions of Henan Province (2021GGJS081).

Notes

The authors declare no competing financial interest.

REFERENCES

(1) Smushkin, G.; Vella, A. What is type 2 diabetes? *Medicine* **2010**, *38*, 597−601.
(2) Chen, H. H.; Nie, Q. X.; Hu, J. L.; Huang, X. J.; Zhang, K.; Pan, S. J.; Nie, S. P. Hypoglycemic and hypolipidemic effects of glucomannan extracted from konjac on type 2 diabetic rats. *J. Agric. Food Chem.* **2019**, *67*, 5278−5288.
(3) Cho, N.H.; Shaw, J.E.; Karuranga, S.; Huang, Y.; da Rocha Fernandes, J.D.; Ohlrogge, A.W.; Malanda, B. IDF Diabetes Atlas: Global estimates of diabetes prevalence for 2017 and projections for 2045. *Diabetes Res. Clin. Pract.* **2018**, *138*, 271−281.
(4) Zhang, C. C.; Geng, C. A.; Huang, X. Y.; Zhang, X. M.; Chen, J. J. Antidiabetic stilbenes from peony seeds with PTP1B, α-glucosidase, and DPPIV inhibitory activities. *J. Agric. Food Chem.* **2019**, *67*, 6765−6772.
(5) Shams Eldin, S. M.; Radwan, M. M.; Wanas, A. S.; Habib, A. M.; Kassem, F. F.; Hammoda, H. M.; Khan, S. I.; Klein, M. L.; Elokely, K. M.; ElSohly, M. A. Bioactivity-guided isolation of potential antidiabetic and antihyperlipidemic compounds from *Trigonella stellata*. *J. Nat. Prod.* **2018**, *81*, 1154−1161.
(6) Ren, Y. X.; Li, L.; Wan, L.; Huang, Y.; Cao, S. Glucokinase as an emerging anti-diabetes target and recent progress in the development of its agonists. *J. Enzyme Inhib. Med. Chem.* **2022**, *37*, 606−615.
(7) Makhoba, X. H.; Viegas, C. J.; Mosa, R. A.; Viegas, F. P. D.; Pooe, O. J. Potential impact of the multi-target drug approach in the treatment of some complex diseases. *Drug Des. Devel. Ther.* **2020**, *14*, 3235−3249.
(8) Xu, L. N.; Li, Y.; Dai, Y.; Peng, J. Y. Natural products for the treatment of type 2 diabetes mellitus: Pharmacology and mechanisms. *Pharmacol. Res.* **2018**, *130*, 451−465.
(9) Zhou, Z. Q.; Fan, H. X.; He, R. R.; Xiao, J.; Tsoi, B.; Lan, K. H.; Kurihara, H.; So, K. F.; Yao, X. S.; Gao, H. Lycibarbarspermidines A-O, new dicaffeoylspermidine derivatives from Wolfberry, with activities against Alzheimer's disease and oxidation. *J. Agric. Food Chem.* **2016**, *64*, 2223−2237.
(10) Gao, Y. J.; Wei, Y. F.; Wang, Y. Q.; Gao, F.; Chen, Z. G. *Lycium barbarum*: A traditional Chinese herb and a promising anti-aging agent. *Aging Dis.* **2017**, *8*, 778−791.
(11) Ma, Z. F.; Zhang, H. X.; Teh, S. S.; Wang, C. W.; Zhang, Y. T.; Hayford, F.; Wang, L. Y.; Ma, T.; Dong, Z. H.; Zhang, Y.; Zhu, Y. F. Goji Berries as a potential natural antioxidant medicine: An insight into their molecular mechanisms of action. *Oxid. Med. Cell. Longev.* **2019**, *2019*, 2437397.
(12) Guo, L.; Du, Q. Q.; Cheng, P. Q.; Yang, T. T.; Xing, C. Q.; Luo, X. Z.; Peng, X. C.; Qian, F.; Huang, J. R.; Tang, F. R. Neuroprotective effects of *Lycium barbarum* berry on neurobehavioral changes and neuronal loss in the hippocampus of mice exposed to acute ionizing radiation. *Dose Response.* **2021**, *19*, 15593258211057768.
(13) Liu, H.; Cui, B.; Zhang, Z. Mechanism of glycometabolism regulation by bioactive compounds from the fruits of *Lycium barbarum*: A review. *Food Res. Int.* **2022**, *159*, 111408.
(14) Tang, W. M.; Chan, E.; Kwok, C. Y.; Lee, Y. K.; Wu, J. H.; Wan, C. W.; Chan, R. Y.; Yu, P. H.; Chan, S. W. A review of the anticancer and immunomodulatory effects of *Lycium barbarum* fruit. *Inflammopharmacology.* **2012**, *20*, 307−314.
(15) Qian, D.; Zhao, Y. X.; Yang, G.; Huang, L. Q. Systematic review of chemical constituents in the genus *Lycium* (Solanaceae). *Molecules.* **2017**, *22*, 911.
(16) Yu, Z. L.; Xia, M. Q.; Lan, J. P.; Yang, L.; Wang, Z. T.; Wang, R.; Tao, H. X.; Shi, Y. H. A comprehensive review on the ethnobotany, phytochemistry, pharmacology and quality control of the genus *Lycium* in China. *Food Funct.* **2023**, *14*, 2998−3025.
(17) Zhou, Z. Q.; Xiao, J.; Fan, H. X.; Yu, Y.; He, R. R.; Feng, X. L.; Kurihara, H.; So, K. F.; Yao, X. S.; Gao, H. Polyphenols from wolfberry and their bioactivities. *Food Chem.* **2017**, *214*, 644−654.
(18) Zhou, Z.-Q.; Fan, H.-X.; He, R.-R.; Xiao, J.; Tsoi, B.; Lan, K.-H.; Kurihara, H.; So, K.-F.; Yao, X.-S.; Gao, H. Lycibarbarspermidines A-O, new dicaffeoylspermidine derivatives from Wolfberry, with activities against Alzheimer's disease and oxidation. *J. Agric. Food Chem.* **2016**, *64*, 2223−2237.
(19) Huang, K. Y.; Dong, W.; Liu, W. Y.; Yan, Y. M.; Wan, P.; Peng, Y. J.; Xu, Y. J.; Zeng, X. X.; Cao, Y. L. 2-*O*-β-D-glucopyranosyl-L-ascorbic acid, an ascorbic acid derivative isolated from the fruits of *Lycium Barbarum* L., modulates gut microbiota and palliates colitis in dextran sodium sulfate-induced colitis in mice. *J. Agric. Food Chem.* **2019**, *67*, 11408−11419.
(20) Tian, X. J.; Liang, T. S.; Liu, Y. L.; Ding, G. T.; Zhang, F. M.; Ma, Z. R. Extraction, structural characterization, and biological functions of *Lycium Barbarum* polysaccharides: A review. *Biomolecules.* **2019**, *9*, 389.
(21) Masci, A.; Carradori, S.; Casadei, M. A.; Paolicelli, P.; Petralito, S.; Ragno, R.; Cesa, S. *Lycium barbarum* polysaccharides: Extraction, purification, structural characterisation and evidence about hypoglycaemic and hypolipidaemic effects. A review. *Food Chem.* **2018**, *254*, 377−389.
(22) Gao, K.; Ma, D.; Cheng, Y.; Tian, X.; Lu, Y.; Du, X.; Tang, H.; Chen, J. Three new dimers and two monomers of phenolic amides from the fruits of *Lycium barbarum* and their antioxidant activities. *J. Agric. Food Chem.* **2015**, *63*, 1067−1075.
(23) Wang, S. Y.; Suh, J. H.; Zheng, X.; Wang, Y.; Ho, C. T. Identification and quantification of potential anti-inflammatory hydroxycinnamic acid amides from Wolfberries, fruits of *Lycium barbarum*. *J. Agric. Food Chem.* **2017**, *65*, 364−372.
(24) Zhu, P. F.; Dai, Z.; Wang, B.; Wei, X.; Yu, H. F.; Yan, Z. R.; Zhao, X. D.; Liu, Y. P.; Luo, X. D. The anticancer activities phenolic

amides from the stem of *Lycium barbarum*. *Nat. Prod. Bioprospect.* **2017**, *7*, 421−431.
(25) Zhu, P. F.; Zhao, Y. L.; Dai, Z.; Qin, X. J.; Yuan, H. L.; Jin, Q.; Wang, Y. F.; Liu, Y. P.; Luo, X. D. Phenolic amides with immunomodulatory activity from the nonpolysaccharide fraction of *Lycium barbarum* fruits. *J. Agric. Food Chem.* **2020**, *68*, 3079−3087.
(26) Chen, H.; Kong, J. B.; Zhang, L.; Wang, H. H.; Cao, Y. G.; Zeng, M. N.; Li, M.; Sun, Y. J.; Du, K.; Xue, G. M.; Wu, Y.; Zheng, X. K.; Feng, W. S. Lycibarbarines A-C, three tetrahydroquinoline alkaloids possessing a spiro-heterocycle moiety from the fruits of *Lycium barbarum*. *Org. Lett.* **2021**, *23*, 858−862.
(27) Chen, H.; Li, Y. J.; Sun, Y. J.; Gong, J. H.; Du, K.; Zhang, Y. L.; Su, C. F.; Han, Q. Q.; Zheng, X. K.; Feng, W. S. Lignanamides with potent antihyperlipidemic activities from the root bark of *Lycium chinense*. *Fitoterapia* **2017**, *122*, 119−125.
(28) Li, N.; Zhu, H. T.; Wang, D.; Zhang, M.; Yang, C. R.; Zhang, Y. J. New flavoalkaloids with potent α-glucosidase and acetylcholinesterase inhibitory activities from Yunnan black tea 'Jin-Ya'. *J. Agric. Food Chem.* **2020**, *68*, 7955−7963.
(29) Zhang, C. C.; Geng, C. A.; Huang, X. Y.; Zhang, X. M.; Chen, J. J. Antidiabetic stilbenes from Peony seeds with PTP1B, α-glucosidase, and DPPIV inhibitory activities. *J. Agric. Food Chem.* **2019**, *67*, 6765−6772.
(30) Xie, Z. S.; Gao, G.; Wang, H.; Li, E. W.; Yuan, Y.; Xu, J. Y.; Zhang, Z. Q.; Wang, P.; Fu, Y.; Zeng, H. H.; Song, J. Y.; Hölscher, C.; Chen, H. Dehydroabietic acid alleviates high fat diet-induced insulin resistance and hepatic steatosis through dual activation of PPAR-γ and PPAR-α. *Biomed. Pharmacother.* **2020**, *127*, 110155.
(31) Sakakibara, I.; Ikeya, Y.; Hayashi, K.; Okada, M.; Maruno, M. Three acyclic bis-phenylpropane lignanamides from fruits of *Cannabis sativa*. *Phytochemistry* **1995**, *38*, 1003−1007.
(32) Sakakibara, I.; Katsuhara, T.; Ikeya, Y.; Hayashi, K.; Mitsuhashi, H. Cannabisin A, an arylnaphthalene lignanamide from fruits of *Cannabis sativa*. *Phytochemistry* **1991**, *30*, 3013−3016.
(33) Li, C. X.; Song, X. Y.; Zhao, W. Y.; Yao, G. D.; Lin, B.; Huang, X. X.; Li, L. Z.; Song, S. J. Characterization of enantiomeric lignanamides from *Solanum nigrum* L. and their neuroprotective effects against MPP^+-induced SH-SY5Y cells injury. *Phytochemistry* **2019**, *161*, 163−171.
(34) Liao, S. G.; Wu, Y.; Yue, J. M. Lignans from *Wikstroemia hainanensis*. *Helv. Chim. Acta* **2006**, *89*, 73−80.
(35) Matsuda, N.; Kikuchi, M. Studies on the constituents of *Lonicera* species. X. Neolignan glycosides from the leaves of *Lonicera gracilipes* var. glandulosa Maxim. *Chem. Pharm. Bull.* **1996**, *44*, 1676−1679.
(36) Gan, M. L.; Zhang, Y. L.; Lin, S.; Liu, M. T.; Song, W. X.; Zi, J. C.; Yang, Y. C.; Fan, X. N.; Shi, J. G.; Hu, J. F.; Sun, J. D.; Chen, N. H. Glycosides from the root of *Iodes cirrhosa*. *J. Nat. Prod.* **2008**, *71*, 647−654.
(37) Lee, S.; Kim, C. S.; Yu, J. S.; Kang, H.; Yoo, M. J.; Youn, U. J.; Ryoo, R.; Bae, H. Y.; Kim, K. H. Ergopyrone, a styrylpyrone-fused steroid with a hexacyclic 6/5/6/6/6/5 skeleton from a mushroom *Gymnopilus orientispectabilis*. *Org. Lett.* **2021**, *23*, 3315−3319.
(38) Liu, Y.; Zhang, X. J.; Kelsang, N.; Tu, G. Z.; Kong, D. X.; Lu, J. H.; Zhang, Y. T.; Liang, H.; Tu, P. F.; Zhang, Q. Y. Structurally diverse cytotoxic dimeric chalcones from *Oxytropis chiliophylla*. *J. Nat. Prod.* **2018**, *81*, 307−315.
(39) Okazaki, Y.; Ishizuka, A.; Ishihara, A.; Nishioka, T.; Iwamura, H. New dimeric compounds of avenanthramide phytoalexin in oats. *J. Org. Chem.* **2007**, *72*, 3830−3839.
(40) Zheng, X. H.; Huang, Y. P.; Liang, Q. P.; Xu, W.; Lan, T.; Zhou, G. X. A new lignanamide from the root of *Lycium yunnanense* Kuang and its antioxidant activity. *Molecules* **2018**, *23*, 770−777.
(41) Guntern, A.; Ioset, J.-R.; Queiroz, E. F.; Sándor, P.; Foggin, C. M.; Hostettmann, K. Heliotropamide, a novel oxopyrrolidine-3-carboxamide from *Heliotropium ovalifolium*. *J. Nat. Prod.* **2003**, *66*, 1550−1553.
(42) King, R. R.; Calhoun, L. A. Characterization of cross-linked hydroxycinnamic acid amides isolated from potato common scab lesions. *Phytochemistry* **2005**, *66*, 2468−2473.
(43) Yan, X.; Tang, J.; dos Santos Passos, C.; Nurisso, A.; Simoes-Pires, C. A.; Ji, M.; Lou, H.; Fan, P. Characterization of lignanamides from Hemp (*Cannabis sativa L.*) seed and their antioxidant and acetylcholinesterase inhibitory activities. *J. Agric. Food Chem.* **2015**, *63*, 10611−10619.
(44) Wang, W. X.; Snooks, H. D.; Sang, S. M. The chemistry and health benefits of dietary phenolamides. *J. Agric. Food Chem.* **2020**, *68*, 6248−6267.
(45) Leonard, W. L.; Zhang, P. Z.; Ying, D. Y.; Fang, Z. X. Lignanamides: sources, biosynthesis and potential health benefits - a minireview. *Crit. Rev. Food Sci. Nutr.* **2021**, *61*, 1404−1414.
(46) Davin, L. B.; Jourdes, M.; Patten, A. M.; Kim, K. W.; Vassão, D. G.; Lewis, N. G. Dissection of lignin macromolecular configuration and assembly: Comparison to related biochemical processes in allyl/propenyl phenol and lignin biosynthesis. *Nat. Prod. Rep.* **2008**, *25*, 1015−1090.
(47) Messiano, G. B.; da Silva, T.; Nascimento, I. R.; Lopes, L. M.X. Biosynthesis of antimalarial lignans from *Holostylis reniformis*. *Phytochemistry* **2009**, *70*, 590−596.
(48) Li, Y. Z.; Huang, J.; Gong, Z.; Tian, X. Q. A novel norlignan and a novel phenylpropanoid from *Peperomia tetraphylla*. *Helv. Chim. Acta* **2007**, *90*, 2222−2226.
(49) Li, S. G.; Huang, X. J.; Li, M. M.; Liu, Q.; Liu, H.; Wang, Y.; Ye, W. C. Multiflorumisides A-G, dimeric stilbene glucosides with rare coupling patterns from the roots of *Polygonum multiflorum*. *J. Nat. Prod.* **2018**, *81*, 254−263.
(50) Nishioka, T.; Watanabe, J.; Kawabata, J.; Niki, R. Isolation and activity of *N-p*-coumaroyltyramine, an α-glucosidase inhibitor in Welsh onion (*Allium fistulosum*). *Biosci. Biotechnol. Biochem.* **1997**, *61*, 1138−1141.

https://doi.org/10.1021/acs.jafc.3c01669
J. Agric. Food Chem. XXXX, XXX, XXX−XXX